### Statistics

Comparisons between two groups were performed using the paired or unpaired *t* test. Values of $P < 0.05$ were considered statistically significant. All summarized data are expressed as means ± SEM.

We thank Dr. Andrew Moorhouse (The University of New South Wales, Sydney, Australia) for critical reading of this manuscript. We also thank Dr. Takeharu Nishimoto and Dr. Hideo Nishitani (Kyushu University, Fukuoka, Japan) for useful discussions of this study.

This work was supported, in part, by a Grant-in-Aid for Scientific Research (17590196) and Priority Areas (13142210) from the Ministry of Education, Culture, Sports, Science and Technology of Japan and the Japan Heart Foundation and by a grant from the National Institutes of Health/National Institute of Neurological Disorder and Stroke (NS38126).

Submitted: 24 August 2005
Accepted: 17 February 2006

## References

Alessi, D.R., M. Andjelkovic, B. Caudwell, P. Cron, N. Morrice, P. Cohen, and B.A. Hemmings. 1996. Mechanism of activation of protein kinase B by insulin and IGF-1. *EMBO J.* 15:6541–6551.

Benn, S.C., and C.J. Woolf. 2004. Adult neuron survival strategies–slamming on the brakes. *Nat. Rev. Neurosci.* 5:686–700.

Boyd, J.G., and T. Gordon. 2003. Neurotrophic factors and their receptors in axonal regeneration and functional recovery after peripheral nerve injury. *Mol. Neurobiol.* 27:277–324.

Brewer, G.J. 1995. Serum-free B27/neurobasal medium supports differentiated growth of neurons from the striatum, substantia nigra, septum, cerebral cortex, cerebellum, and dentate gyrus. *J. Neurosci. Res.* 42:674–683.

Brewer, G.J., J.R. Torricelli, E.K. Evege, and P.J. Price. 1993. Optimized survival of hippocampal neurons in B27-supplemented Neurobasal, a new serum-free medium combination. *J. Neurosci. Res.* 35:567–576.

Cantley, L.C. 2002. The phosphoinositide 3-kinase pathway. *Science.* 296:1655–1657.

Chen, X.L., Z.G. Zhong, S. Yokoyama, C. Bark, B. Meister, P.O. Berggren, J. Roder, H. Higashida, and A. Jeromin. 2001. Overexpression of rat neuronal calcium sensor-1 in rodent NG108-15 cells enhances synapse formation and transmission. *J. Physiol.* 532:649–659.

Cheng, A., S. Wang, D. Yang, R. Xiao, and M.P. Mattson. 2003. Calmodulin mediates brain-derived neurotrophic factor cell survival signaling upstream of Akt kinase in embryonic neocortical neurons. *J. Biol. Chem.* 278:7591–7599.

Currie, R.A., K.S. Walker, A. Gray, M. Deak, A. Casamayor, C.P. Downes, P. Cohen, D.R. Alessi, and J. Lucocq. 1999. Role of phosphatidylinositol 3,4,5-trisphosphate in regulating the activity and localization of 3-phosphoinositide-dependent protein kinase-1. *Biochem. J.* 337:575–583.

Gomez, M., E. De Castro, E. Guarin, H. Sasakura, A. Kuhara, I. Mori, T. Bartfai, C.I. Bargmann, and P. Nef. 2001. $Ca^{2+}$ signaling via the neuronal calcium sensor-1 regulates associative learning and memory in *C. elegans*. *Neuron.* 30:241–248.

Henderson, C.E., H.S. Phillips, R.A. Pollock, A.M. Davies, C. Lemeulle, M. Armanini, L. Simmons, B. Moffet, R.A. Vandlen, L.C. Simpson, et al. 1994. GDNF: a potent survival factor for motoneurons present in peripheral nerve and muscle. *Science.* 266:1062–1064.

Hendricks, K.B., B.Q. Wang, E.A. Schnieders, and J. Thorner. 1999. Yeast homologue of neuronal frequenin is a regulator of phosphatidylinositol-4-OH kinase. *Nat. Cell Biol.* 1:234–241.

Jeromin, A., A.J. Shayan, M. Msghina, J. Roder, and H.L. Atwood. 1999. Crustacean frequenins: molecular cloning and differential localization at neuromuscular junctions. *J. Neurobiol.* 41:165–175.

Jeromin, A., D. Muralidhar, M.N. Parameswaran, J. Roder, T. Fairwell, S. Scarlata, L. Dowal, S.M. Mustafi, K.V. Chary, and Y. Sharma. 2004. N-terminal myristoylation regulates calcium-induced conformational changes in neuronal calcium sensor-1. *J. Biol. Chem.* 279:27158–27167.

Kakizawa, S., M. Yamasaki, M. Watanabe, and M. Kano. 2000. Critical period for activity-dependent synapse elimination in developing cerebellum. *J. Neurosci.* 20:4954–4961.

Kirik, D., B. Georgievska, and A. Bjorklund. 2004. Localized striatal delivery of GDNF as a treatment for Parkinson disease. *Nat. Neurosci.* 7:105–110.

Kiryu-Seo, S., M. Sasaki, H. Yokohama, S. Nakagomi, T. Hirayama, S. Aoki, K. Wada, and H. Kiyama. 2000. Damage-induced neuronal endopeptidase (DINE) is a unique metallopeptidase expressed in response to neuronal damage and activates superoxide scavengers. *Proc. Natl. Acad. Sci. USA.* 97:4345–4350.

Koh, P.O., A.S. Undie, N. Kabbani, R. Levenson, P.S. Goldman-Rakic, and M.S. Lidow. 2003. Up-regulation of neuronal calcium sensor-1 (NCS-1) in the prefrontal cortex of schizophrenic and bipolar patients. *Proc. Natl. Acad. Sci. USA.* 100:313–317.

Koizumi, S., P. Rosa, G.B. Willars, R.A. Challiss, E. Taverna, M. Francolini, M.D. Bootman, P. Lipp, K. Inoue, J. Roder, and A. Jeromin. 2002. Mechanisms underlying the neuronal calcium sensor-1-evoked enhancement of exocytosis in PC12 cells. *J. Biol. Chem.* 277:30315–30324.

Korhonen, L., I. Hansson, J.P. Kukkonen, K. Brannvall, M. Kobayashi, K. Takamatsu, and D. Lindholm. 2005. Hippocalcin protects against caspase-12-induced and age-dependent neuronal degeneration. *Mol. Cell. Neurosci.* 28:85–95.

Liberatore, G.T., J.Y. Wong, M.J. Porritt, G.A. Donnan, and D.W. Howells. 1997. Expression of glial cell line-derived neurotrophic factor (GDNF) mRNA following mechanical injury to mouse striatum. *Neuroreport.* 8:3097–3101.

Liston, P., W.G. Fong, and R.G. Korneluk. 2003. The inhibitors of apoptosis: there is more to life than Bcl2. *Oncogene.* 22:8568–8580.

Mallart, A., D. Angaut-Petit, C. Bourret-Poulain, and A. Ferrus. 1991. Nerve terminal excitability and neuromuscular transmission in T(X;Y)V7 and Shaker mutants of *Drosophila melanogaster*. *J. Neurogenet.* 7:75–84.

Mercer, E.A., L. Korhonen, Y. Skoglosa, P.A. Olsson, J.P. Kukkonen, and D. Lindholm. 2000. NAIP interacts with hippocalcin and protects neurons against calcium-induced cell death through caspase-3-dependent and -independent pathways. *EMBO J.* 19:3597–3607.

Nabekura, J., T. Ueno, S. Katsurabayashi, A. Furuta, N. Akaike, and M. Okada. 2002a. Reduced NR2A expression and prolonged decay of NMDA receptor-mediated synaptic current in rat vagal motoneurons following axotomy. *J. Physiol.* 539:735–741.

Nabekura, J., T. Ueno, A. Okabe, A. Furuta, T. Iwaki, C. Shimizu-Okabe, A. Fukuda, and N. Akaike. 2002b. Reduction of KCC2 expression and GABAA receptor-mediated excitation after in vivo axonal injury. *J. Neurosci.* 22:4412–4417.

Nakamura, T.Y., D.J. Pountney, A. Ozaita, S. Nandi, S. Ueda, B. Rudy, and W.A. Coetzee. 2001. A role for frequenin, a $Ca^{2+}$-binding protein, as a regulator of Kv4 $K^+$-currents. *Proc. Natl. Acad. Sci. USA.* 98:12808–12813.

Nakamura, T.Y., E. Sturm, D.J. Pountney, B. Orenzoff, M. Artman, and W.A. Coetzee. 2003. Developmental expression of NCS-1 (frequenin), a regulator of Kv4 $K^+$ channels, in mouse heart. *Pediatr. Res.* 53:554–557.

Nicole, O., C. Ali, F. Docagne, L. Plawinski, E.T. MacKenzie, D. Vivien, and A. Buisson. 2001. Neuroprotection mediated by glial cell line-derived neurotrophic factor: involvement of a reduction of NMDA-induced calcium influx by the mitogen-activated protein kinase pathway. *J. Neurosci.* 21:3024–3033.

Olafsson, P., T. Wang, and B. Lu. 1995. Molecular cloning and functional characterization of the *Xenopus* $Ca^{2+}$-binding protein frequenin. *Proc. Natl. Acad. Sci. USA.* 92:8001–8005.

Oppenheim, R.W., L.J. Houenou, J.E. Johnson, L.F. Lin, L. Li, A.C. Lo, A.L. Newsome, D.M. Prevette, and S. Wang. 1995. Developing motor neurons rescued from programmed and axotomy-induced cell death by GDNF. *Nature.* 373:344–346.

Perez-Garcia, M.J., V. Cena, Y. de Pablo, M. Llovera, J.X. Comella, and R.M. Soler. 2004. Glial cell line-derived neurotrophic factor increases intracellular calcium concentration. Role of calcium/calmodulin in the activation of the phosphatidylinositol 3-kinase pathway. *J. Biol. Chem.* 279:6132–6142.

Perrelet, D., A. Ferri, P. Liston, P. Muzzin, R.G. Korneluk, and A.C. Kato. 2002. IAPs are essential for GDNF-mediated neuroprotective effects in injured motor neurons in vivo. *Nat. Cell Biol.* 4:175–179.

Pongs, O., J. Lindemeier, X.R. Zhu, T. Theil, D. Engelkamp, I. Krah-Jentgens, H.G. Lambrecht, K.W. Koch, J. Schwemer, R. Rivosecchi, et al. 1993. Frequenin–a novel calcium-binding protein that modulates synaptic efficacy in the *Drosophila* nervous system. *Neuron.* 11:15–28.

Rothstein, J.D., S. Patel, M.R. Regan, C. Haenggeli, Y.H. Huang, D.E. Bergles, L. Jin, M. Dykes Hoberg, S. Vidensky, D.S. Chung, et al. 2005. Beta-lactam antibiotics offer neuroprotection by increasing glutamate transporter expression. *Nature.* 433:73–77.

Sippy, T., A. Cruz-Martin, A. Jeromin, and F.E. Schweizer. 2003. Acute changes in short-term plasticity at synapses with elevated levels of neuronal calcium sensor-1. *Nat. Neurosci.* 6:1031–1038.

Soler, R.M., X. Dolcet, M. Encinas, J. Egea, J.R. Bayascas, and J.X. Comella. 1999. Receptors of the glial cell line-derived neurotrophic factor family of neurotrophic factors signal cell survival through the phosphatidylinositol 3-kinase pathway in spinal cord motoneurons. *J. Neurosci.* 19:9160–9169.

Takahashi, M. 2001. The GDNF/RET signaling pathway and human diseases. *Cytokine Growth Factor Rev.* 12:361–373.

Tsujimoto, T., A. Jeromin, N. Saitoh, J.C. Roder, and T. Takahashi. 2002. Neuronal calcium sensor 1 and activity-dependent facilitation of P/Q-type calcium currents at presynaptic nerve terminals. *Science.* 295:2276–2279.

Wang, C.Y., F. Yang, X. He, A. Chow, J. Du, J.T. Russell, and B. Lu. 2001. $Ca^{2+}$ binding protein frequenin mediates GDNF-induced potentiation of $Ca^{2+}$ channels and transmitter release. *Neuron.* 32:99–112.

Wang, Y., C.F. Chang, M. Morales, Y.H. Chiang, and J. Hoffer. 2002. Protective effects of glial cell line-derived neurotrophic factor in ischemic brain injury. *Ann. NY Acad. Sci.* 962:423–437.

Weiss, J.L., D.A. Archer, and R.D. Burgoyne. 2000. Neuronal $Ca^{2+}$ sensor-1/frequenin functions in an autocrine pathway regulating $Ca^{2+}$ channels in bovine adrenal chromaffin cells. *J. Biol. Chem.* 275:40082–40087.

Weisz, O.A., G.A. Gibson, S.M. Leung, J. Roder, and A. Jeromin. 2000. Overexpression of frequenin, a modulator of phosphatidylinositol 4-kinase, inhibits biosynthetic delivery of an apical protein in polarized madin-darby canine kidney cells. *J. Biol. Chem.* 275:24341–24347.

Yamamoto, M., N. Mitsuma, Y. Ito, N. Hattori, M. Nagamatsu, M. Li, T. Mitsuma, and G. Sobue. 1998. Expression of glial cell line-derived neurotrophic factor and GDNFR-alpha mRNAs in human peripheral neuropathies. *Brain Res.* 809:175–181.

Yan, Q., C. Matheson, and O.T. Lopez. 1995. In vivo neurotrophic effects of GDNF on neonatal and adult facial motor neurons. *Nature.* 373:341–344.

Growth was assayed by measuring the reduction of sodium 2,3-bis-[2-methoxy-4-nitro-5-sulfophenyl]-2*H*-tetrazolium-5-carboxanilide (XTT) [11]. Amphotericin-B was used as positive control [12], and the cell toxicity was assessed by measuring the reduction of XTT by murine macrophages (cell line J744) and VERO cells [13], [14].


## Acknowledgements

This work was supported by US NIH grant #1U01 TW00663401 from the International Cooperative Biodiversity Groups Program ICBG-Panama and by funds from the Smithsonian Tropical Research Institute.


## References


[1] Montenegro H, Gutiérrez M, Romero LI, Ortega-Barría , Capson TL, Cubilla L. Aporphine alkaloids from *Guatteria* spp. with leishmanicidal activity. Planta Med 2003; 69: 677–9

[2] Berman J. Recent developments in leishmaniasis: epidemiology, diagnosis, and treatment. Curr Infect Dis Rep 2005; 7: 33–8

[3] Li D, Zhao B, Sim SP, Li TK, Liu A, Liu LF et al. 2,3-Dimethoxybenzo[*i*]phenanthridines: topoisomerase I-targeting anticancer agents. Bioorg Med Chem 2003; 11: 521–8

[4] Iwasa K, Nishiyama Y, Ichimaru M, Moriyasu M, Kim HS, Wataya Y et al. Structure-activity relationships of quaternary protoberberine alkaloids having an antimalarial activity. Eur J Med Chem 1999; 34: 1077–83

[5] Werbovetz A, Bhattacharjee K, Brendle J, Scovil P. Analysis of stereoelectronic properties of camptothecin analogues in relation to biological activity. Bioorg Med Chem 2000; 8: 1741–7

[6] Guinaudeau H, Leboeuf M, Cave A. Aporphine alkaloids. J Nat Prod 1975; 38: 275–335

[7] Hocquemiller R, Cave A, Raharisololalao A. Alcaloides de *Xylopya buxifolia* et de *Xylopia danguyella*. J Nat Prod 1981; 44: 551–6

[8] Chen CL, Chang HM, Cowling E, Huang CY, Gates R. Aporphine alkaloids and lignans formed in response to injury of sapwood in *Liriodendron tulipifera*. Phytochemistry 1976; 15: 1161–7

[9] Castro O, López J, Vergara A. Aporphine alkaloids from *Phoebe pittieri*. Phytochemistry 1985; 24: 203–4

[10] Gellert E, Summons RE. Alkaloids of the genus *Cinnamomum*. II. Alkaloids of the bark of *Cinnamomum* sp. T.G.H. 13077. Aust J Chem 1970; 23: 2095–9

[11] Williams C, Espinosa OA, Montenegro H, Cubilla L, Capson TL, Ortega-Barría E et al. Hydrosoluble formazan XTT: its application to natural products drug discovery for *Leishmania*. J Microbiol Methods 2003; 55: 813–6

[12] Golenser J, Frankenburg S, Enrenfreund T, Domb AJ. Efficacious treatment of experimental leishmaniasis with amphotericin B-arabinogalactan water-soluble derivatives. Antimicrob Agents Chemother 1999; 43: 2209–14

[13] Shin IS, Tanifuji H, Arata Y, Morizawa Y, Nakayama T, Wataya Y. 3′-Deoxy-3′-fluoroinosine as a potent antileishmanial agent. The metabolism and selective cytotoxic effect of 3′-deoxy-3′-fluoroinosine against *Leishmania tropica* and *L. donovani in vitro* and *in vivo*. Parasitol Res 1995; 81: 622–6

[14] Sahpaz S, Bories C, Loiseau PM, Cortes D, Hocquemiller R, Laurens A et al. Cytotoxic and antiparasitic activity from *Annona senegalensis* seeds. Planta Med 1994; 60: 538–40




# Inhibitory Effects of Ginsenoside-Rb1 on Activation of the 12-*O*-Tetradecanoylphorbol 13-Acetate-Induced Cyclooxygenase-2 Promoter


Wankyu Park[1], Wonchung Lim[1], Jungyoon Cho[1], Hiroyasu Inoue[2], Mee-Ra Rhyu[3], YoungJoo Lee[1]



## Abstract

We studied the inhibitory effects of ginsenoside-Rb1 (1) on 12-*O*-tetradecanoylphorbol 13-acetate (TPA)-induced transcriptional activation of the cyclooxygenase-2 (COX-2) promoter. The suppressive activity of ginsenoside-Rb1 was characterized using COX-2 promoter-driven luciferase reporter plasmids in a transient transfection system. Ginsenoside-Rb1 at 100 μM inhibited TPA-induced transcriptional activation of the COX-2 promoter. To identify the *cis*-acting elements responsible for this inhibition, the effects of site-specific mutations in the COX-2 promoter region were examined. Inhibition by ginsenoside-Rb1 was not affected by mutations in nuclear factor-κB- or cAMP-responsive elements. However, the effects were abolished when the nuclear factor-interleukin-6 binding site was mutated, indicating that ginsenoside-Rb1 exerts its effects via this element. In conclusion, ginsenoside-Rb1 inhibits TPA-induced COX-2 promoter activity through the nuclear factor interleukin-6 binding site and not through the nuclear factor-κB or cAMP-responsive elements.


Ginseng has been used for thousands of years in Asian countries for its wide spectrum of medicinal properties. It has antioxidant, immunomodulatory, antiaging, and anticancer activities [1]. Use of ginseng has expanded to Western countries, and continues to rise with the increasing popularity of complementary and alternative medicine. Although the beneficial effects of ginseng have prompted tremendous efforts to discover the pharmacology of its action through biochemical and molecular biology techniques, a detailed mechanism has yet to be determined.

A number of ginseng components have been isolated and characterized, such as ginsenosides, polysaccharides, peptides, polyacetylenic alcohols, and fatty acids [2]. The major pharmacologically active components of ginseng are the ginsenosides, which are steroidal saponins comprising 3–6% of the total ginseng


**Affiliation:** [1] College of Life Science, Institute of Biotechnology, Department of Bioscience and Biotechnology, Sejong University, Seoul, Korea · [2] Department of Food Science and Nutrition, Faculty of Human Life and Environment, Nara Women's University, Nara, Japan · [3] Food Function Research Division, Korea Food Research Institute, Gyeonggi-Do, Korea

**Correspondence:** YoungJoo Lee, Ph. D. · Department of Bioscience and Biotechnology · Sejong University · Kwang-Jin-Gu · Seoul 143–747 · Korea · Phone: +82-2-3408-3766 · Fax: +82-2-3408-3334 · E-mail: yjlee@sejong.ac.kr



**Received:** January 14, 2005 · **Accepted:** August 3, 2005

**Bibliography:** Planta Med 2006; 72: 272–275 © Georg Thieme Verlag KG Stuttgart · New York · DOI 10.1055/s-2005-873172 · Published online November 10, 2005 · ISSN 0032-0943

mass [3]. In particular, ginseng extracts contain 0.4–1.8% ginsenoside-Rb1 (**1**; Fig. **1**) by weight, depending on manufacturing and processing methods, which belongs to the protopanaxadiol class of ginsenosides [4]. Studies on the activity of ginsenoside-Rb1 have demonstrated effects on cardiac contraction, adrenal hydroxylase upregulation, and estrogenicity [5], [6], [7], [8].

Cyclooxygenase (prostaglandin H synthase; COX) is a key regulatory enzyme in the conversion of arachidonic acid to prostaglandins. It is found as two distinct isoforms: COX-1 is expressed constitutively in most tissues and COX-2 is inducible by extracellular stimuli such as tumor promoters, proinflammatory cytokines and growth factors [9], [10]. Several studies have indicated that induction of COX-2 expression is important in inflammation, immune responsivity, and carcinogenesis [11], [12]. Transcriptional activation of COX-2 is regulated by the binding of transcription factors to the COX-2 promoter, which contains multiple putative *cis*-acting elements for transcription factors. These elements include a cAMP-responsive element (CRE), an E-box, binding sites for nuclear factor (NF)-κB, NF-interleukin-6 (NF-IL6), and activator protein 2 (AP2). The consensus *cis*-acting sites of NF-kB, NF-IL6, and CRE are of major importance in hormone-, cytokine-, and tumor promoter-stimulated responses [13], [14], [15].

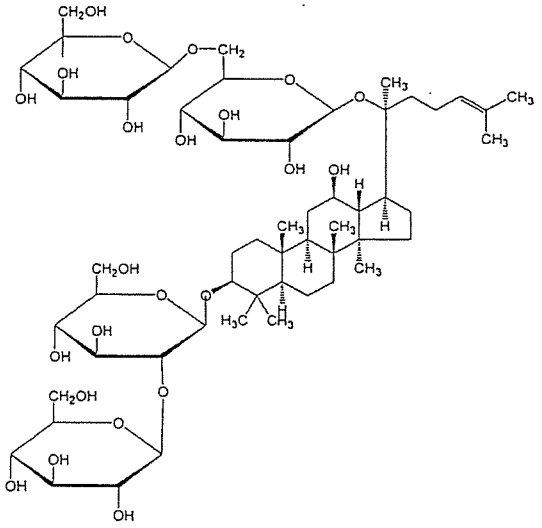

Fig. 1 The structure of ginsenoside-Rb1 (**1**).

In the present study, we examined the inhibition of 12-*O*-tetradecanoylphorbol 13-acetate (TPA)-induced COX-2 promoter activation by ginsenoside-Rb1, as well as the specific promoter binding sites involved in this process. The data, which were obtained using a COX-2 promoter-reporter system, demonstrate that ginsenoside-Rb1 has an inhibitory effect on the transcriptional activity of the TPA-induced COX-2 promoter, and that this inhibition is mediated through the NF-IL6 element.

A luciferase reporter gene under control of the full-length mouse COX-2 promoter was transiently transfected into COS cells, and the cells were exposed to 10 nM TPA with or without ginsenoside-Rb1 for 24 h. Treatment of cells with ginsenoside-Rb1 alone had no effect on luciferase activity driven by the COX-2 promoter. However, simultaneous treatment with TPA and ginsenoside-Rb1 decreased luciferase activity as compared to cells treated with TPA alone in a concentration-dependent manner (Figs. **2A** and **B**). These results suggest that ginsenoside-Rb1 inhibits TPA-induced COX-2 promoter activation. It is well known that another tumor promoter such as tumor necrosis factor α (TNFα) induces COX-2 [16]. As shown in Fig. **2C**, ginsenoside-Rb1 also inhibits TNFα-induced COX-2 promoter activation.

The 5′-flanking region of the COX-2 promoter (−327/+59) contains an NF-κB binding site (−223/−214), an NF-IL6 binding site (−132/−124), and a CRE (−59/−53) binding site [17]. To identify the region(s) involved in ginsenoside-Rb1-mediated COX-2 promoter inhibition, we transiently transfected reporter constructs containing mutations in either the NF-κB (KBM) or both the NF-IL6 and CRE (ILM/CRM) sites into COS cells. As shown in Fig. **3A**, the inhibitory effects of ginsenoside-Rb1 on TPA-induced COX-2 promoter activity were retained in cells transfected with the KBM reporter gene, indicating that NF-κB is not involved in ginsenoside-Rb1-mediated inhibition of COX-2 promoter activity. In contrast, ginsenoside-Rb1 had no inhibitory effect in cells transfected with the ILM/CRM reporter genes (Fig. **3B**). Furthermore, mutations in the NF-IL6 site (−132/−124) abolished ginsenoside-Rb1-mediated inhibition as compared to the effects on the full-length mouse COX-2 promoter (Fig. **4A**). These results suggest that ginsenoside-Rb1 exerts its inhibitory effects on COX-2 promoter activity via the NF-IL6 site. The relative lack of importance of the CRE and NF-κB sites in eliciting the ginsenoside-Rb1-mediated response was confirmed by experiments in which

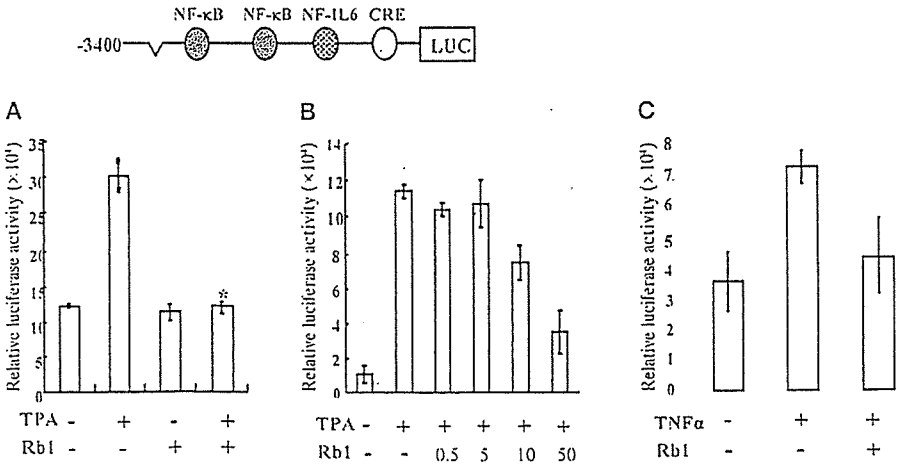


Fig. 2 Ginsenoside-Rb1 inhibits TPA-induced COX-2 promoter transcription activity. Cells were transiently transfected with the full length 3.4 kb COX-2 promoter and treated with 10 nM TPA and 100 μM of ginsenoside-Rb1 (A), 10 nM TPA with increasing concentrations of ginsenoside-Rb1 (B), or 10 ng/mL TNFα with ginsenoside-Rb1 (C) as indicated for 24 h, then assayed for luciferase activity as described in Materials and Methods. Transfections were performed in triplicate. One representative result is shown in this figure. Data are expressed as the mean ± S.E.M.

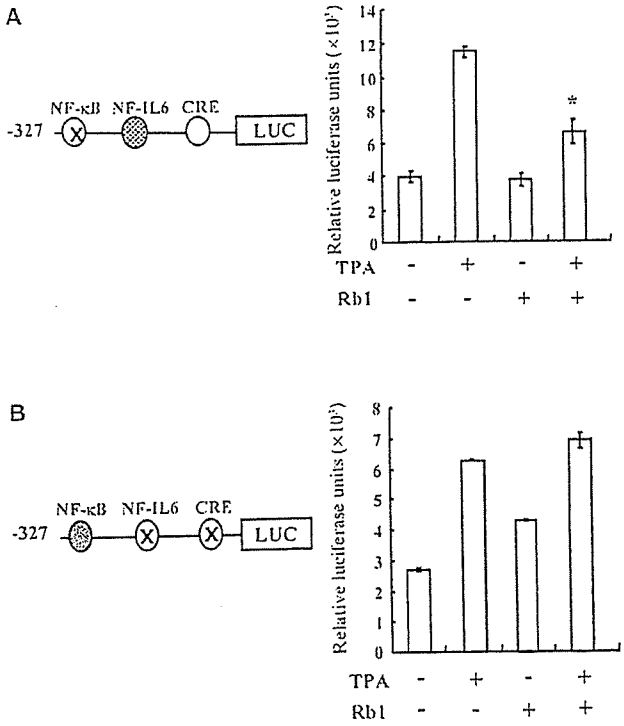


Fig. 3 NF-κB is not involved in ginsenoside-Rb1-mediated inhibition on TPA-induced COX-2 promoter activity. Cells were transiently transfected with KBM (A) or ILM/CRM (B) reporter gene, treated with 10 nM TPA and 100 μM ginsenoside-Rb1, and assayed for luciferase activity after 24 h of treatment. Data are representative of least three independent experiments performed in triplicate.

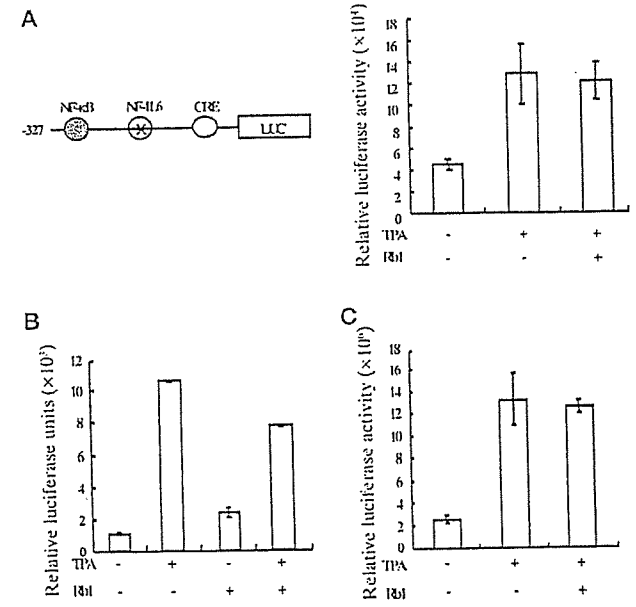


Fig. 4 The NF-IL6 site is responsible for ginsenoside-Rb1-mediated inhibition on TPA-induced COX-2 promoter activity. Cells were transiently transfected with ILM (A), or $p(CRE)_5$ (B), or $p(NF\text{-}\kappa B)_7$ (C) reporter gene and treated with of 10 nM TPA and 100 μM ginsenoside-Rb1 for 24 h. Transfections were performed in triplicate more than three times, and one representative dataset is shown.

COS cells were transiently transfected with $p(CRE)_5$-Luc or $p(NF\text{-}\kappa B)_7$-Luc constructs. As shown in Figs. 4B and C, ginsenoside-Rb1 had no significant effect on these cells.

In this study, we examined the effects of ginsenoside-Rb1 on TPA-induced COX-2 promoter activation. In particular, we attempted to identify the COX-2 promoter region that is important for mediating the inhibitory effects of ginsenoside-Rb1 by mutagenizing specific transcription factor binding sites in the COX-2 promoter. Our data indicate that ginsenoside-Rb1 inhibits TPA-induced COX-2 promoter stimulation via the NF-IL6 binding site. NF-IL6 is a pleiotropic transcription factor for numerous genes of cellular differentiation and inflammation such as IL-6, TNF-α, granulocyte colony stimulating factor, COX-2 and inducible nitric oxide synthase [18]. It has been shown that COX-2 expression is regulated through NF-IL6 by staurosporin, sauchinone from *Saurus chinensis*, and aspirin [14], [15], [19]. In addition, NF-IL6 is one of the targets for the COX-2 regulation in many cancer cells [20]. Our results on the effects of ginsenoside-Rb1 on COX-2 implicate the clinical value of ginseng for the treatment of inflammation and tumor growth and provide a mechanistic clue to the antitumor activity of ginseng, although the exact nature of the activity is far from clear. Future studies investigating the effects of ginsenoside-Rb1 on endogenous COX-2 gene expression in various cancer cell lines and in *in vitro* tumor models will be helpful in further elucidating the molecular mechanism of ginsenoside-Rb1-mediated inhibition of TPA-induced COX-2 promoter activation.

## Materials and Methods

Ginsenoside-Rb1, provided by the Korea Ginseng and Tobacco Research Institute (Daejeon, Korea), was dissolved in 20% ethanol at a concentration of 15 mg/mL and added to the medium at 100 μM. An untreated group served as a control. TPA and TNFα were obtained from Sigma and used at 10 nM and 10 ng/mL, respectively.

The mouse COX-2 full promoter luciferase reporter construct was kindly provided by Dr. Hui-Fang Cheng. The human COX-2 promoter driven mutated constructs were cloned as described [17]. The plasmids $p(CRE)_4$-Luc and $p(NF\text{-}\kappa B)_5$-Luc were purchased from Stratagene.

COS cells, a monkey kidney cell line, were maintained in phenol red-free Dulbecco's modified Eagle's medium from Sigma (DMEM) with 10% (vol/vol) calf serum (GIBCO).

Cells were transiently transfected by electroporation as described [21]. Electroporation was performed with a Gene Pulser II (Bio-Rad). Cells were trypsinized, washed in cold PBS, and resuspended in PBS. A 400-μL portion of the suspension was mixed with 20 μg of plasmid DNA. After 5 min at room temperature, cells were pulsed at 1000 μF and 250 V. After 10 min incubation at 37 °C, the suspension was diluted in medium and cultured for 24 h. Cells were replaced with fresh medium and treated for 24 h. After treatment, the cells were harvested and lysed with reporter lysis buffer (Promega Luciferase Assay system). The cell extract was mixed with the luciferase assay reagent, analyzed by the AutoLumat LB953 luminometer and expressed as relative light units. The mean and standard errors of triplicate or quadruplicate samples are shown for representative experiments. All transfection experiments were repeated three or more times with similar results.

Values shown represent mean ± SEM. Statistical analysis was performed by Student's *t* test with a *p* value of less than 0.05 being considered statistically significant.


## Acknowledgements

This work was supported in part by grants from the Korea Tobacco and Ginseng Corp. R&D program 2002, Korean Ministry of Health and Welfare (HMP-00-O-21600-009), and BK21 program to Y. J. Lee.


## References


[1] Attele AS, Wu JA, Yuan CS. Ginseng pharmacology: multiple constituents and multiple actions. Biochem Pharmacol 1999; 58: 1685–93

[2] Liu WK, Xu SX, Che CT. Anti-proliferative effect of ginseng saponins on human prostate cancer cell line. Life Sci 2000; 67: 1297–306

[3] Yoon M, Lee H, Jeong S, Kim JJ, Nicol CJ, Nam KW et al. Peroxisome proliferator-activated receptor alpha is involved in the regulation of lipid metabolism by ginseng. Br J Pharmacol 2003; 138: 1295–302

[4] Shibata S. Chemistry and cancer preventing activities of ginseng saponins and some related triterpenoid compounds. J Korean Med Sci 2001; 16 (Suppl): S28S37

[5] Morschl E, Bretus I, Nemcsik J, Laszlo F, Pavo I. Estrogen-mediated upregulation of the Ca-dependent constitutive nitric oxide synthase in the rat aorta and heart. Life Sci 2000; 68: 49–55

[6] Scott GI, Colligan PB, Ren BH, Ren J. Ginsenosides Rb1 and Re decrease cardiac contraction in adult rat ventricular myocytes: role of nitric oxide. Br J Pharmacol 2001; 134: 1159–65

[7] Kim HS, Zhang YH, Fang LH, Lee MK. Effects of ginsenosides on bovine adrenal tyrosine hydroxylase. J Ethnopharmacol 1999; 66: 107–11

[8] Cho JY, Park WK, Lee SG, Ahn WS, Lee YJ. Ginsenoside-Rb1 from *Panax ginseng* C.A. Meyer activates estrogen receptor-alpha and -beta, independent of ligand binding. J Clin Endocrinol Metab 2004; 89: 3510–5

[9] Funk CD, Funk LB, Kennedy ME, Pong AS, Fitzgerald GA. Human platelet/erythroleukemia cell prostaglandin G/H synthase: cDNA cloning, expression, and gene chromosomal assignment. FASEB J 1991; 5: 2304–12

[10] Smith WL, DeWitt DL, Garavito RM. Cyclooxygenases: structural, cellular, and molecular biology. Annu Rev Biochem 2000; 69: 45–82

[11] Chen CC, Sun YT, Chen JJ, Chiu KT. TNF-alpha-induced cyclooxygenase-2 expression in human lung epithelial cells: involvement of the phospholipase C-gamma 2, protein kinase C-alpha, tyrosine kinase, NF-kappa B-inducing kinase, and I-kappa B kinase 1/2 pathway. J Immunol 2000; 165: 2719–28

[12] Chen Y, Yang L, Lee TJ. Oroxylin A inhibition of lipopolysaccharide-induced iNOS and COX-2 gene expression via suppression of nuclear factor-kappaB activation. Biochem Pharmacol 2000; 59: 1445–57

[13] Sirois J, Levy LO, Simmons DL, Richards JS. Characterization and hormonal regulation of the promoter of the rat prostaglandin endoperoxide synthase 2 gene in granulosa cells. Identification of functional and protein-binding regions. J Biol Chem 1993; 268: 12199–206

[14] Saunders MA, Sansores-Garcia L, Gilroy DW, Wu KK. Selective suppression of CCAAT/enhancer-binding protein beta binding and cyclooxygenase-2 promoter activity by sodium salicylate in quiescent human fibroblasts. J Biol Chem 2001; 276: 18897–904

[15] Wang CY, Lei HJ, Huang CY, Zhang Z, Mukherjee AB, Yuan CJ. Induction of cyclooxygenase-2 by staurosporine through the activation of nuclear factor for IL-6 (NF-IL6) and activator protein 2 (AP2) in an osteoblast-like cell line. Biochem Pharmacol 2002; 64: 177–84

[16] Yamamoto K, Arakawa T, Ueda N, Yamamoto S. Transcriptional roles of nuclear factor κB and nuclear factor-interleukin-6 in the tumor necrosis factor α-dependent induction of cyclooxygenase-2 in MC3T3-E1 cells. J Biol Chem 1995; 270: 31315–20

[17] Inoue H, Umesono K, Nishimori T, Hirata Y, Tanabe T. Glucocorticoid-mediated suppression of the promoter activity of the cyclooxygenase-2 gene is modulated by expression of its receptor in vascular endothelial cells. Biochem Biophys Res Commun 1999; 254: 292–8

[18] Hattori T, Ohoka N, Hayashi H, Onozaki K. C/EBP homologous protein (CHOP) up-regulates IL-6 transcription by trapping negative regulating NF-IL6 isoform. FEBS Lett 2003; 541: 33–9

[19] Lee AK, Sung SH, Kim YC, Kim SG. Inhibition of lipopolysaccharide-inducible nitric oxide synthase, TNF-α and COX-2 expression by sauchinone effects on I-κBa phosphorylation, C/EBP and AP-1 activation. Br J Pharmacol 2003; 139: 11–20

[20] Wardlaw SA, Zhang N, Belinsky SA. Transcriptional regulation of basal cyclooxygenase-2 expression in murine lung tumor-derived cell lines by CCAAT/enhancer-binding protein and activating transcription factor/cAMP response element-binding protein. Mol Pharmacol 2002; 62: 326–33

[21] Faussner A, Bauer A, Kalatskaya I, Jochum M, Fritz H. Expression levels strongly affect ligand-induced sequestration of B2 bradykinin receptors in transfected cells. Am J Physiol Heart Circ Physiol 2003; 284: 1892–8

Acta Crystallographica Section F
**Structural Biology and Crystallization Communications**
ISSN 1744-3091

# Crystallization and preliminary X-ray crystallographic analysis of two vascular apoptosis-inducing proteins (VAPs) from *Crotalus atrox* venom

**Tomoko Igarashi,[a] Yuko Oishi,[a] Satohiko Araki,[b] Hidezo Mori[a] and Soichi Takeda[a,c]***

[a]Department of Cardiac Physiology, National Cardiovascular Center Research Institute, 5-7-1 Fujishiro-dai, Suita, Osaka 565-8565, Japan, [b]Sugashima Marine Biological Laboratory, Graduate School of Science, Nagoya University, Toba, Mie 517-0004, Japan, and [c]Laboratory for Structural Biochemistry, Riken Harima Institute at SPring-8, 1-1-1 Kouto, Mikazuki, Sayo, Hyogo 679-5148, Japan

Correspondence e-mail: stakeda@ri.ncvc.go.jp

Received 11 May 2006
Accepted 12 June 2006

VAPs are haemorrhagic snake-venom toxins belonging to the reprolysin family of zinc metalloproteinases. *In vitro*, VAPs induce apoptosis specifically in cultured vascular endothelial cells. VAPs have a modular structure that bears structural homology to mammalian ADAMs (a disintegrin and metalloproteinases). VAP1 is a homodimer with a MW of 110 kDa in which the monomers are connected by a single disulfide bridge. VAP2 is homologous to VAP1 and exists as a monomer with a MW of 55 kDa. In the current study, several crystal forms of VAP1 and VAP2 were obtained using the vapour-diffusion method and diffraction data sets were collected using SPring-8 beamlines. The best crystals of VAP1 and VAP2 generated data sets to 2.5 and 2.15 Å resolution, respectively.

## 1. Introduction

Haemorrhagic snake venoms contain factors that induce apoptosis specifically in cultured vascular endothelial cells (Araki *et al.*, 1993). The vascular apoptosis-inducing proteins VAP1 and VAP2 were originally isolated from the venom of the western diamondback rattlesnake *Crotalus atrox* (Masuda *et al.*, 1997, 1998) and similar apoptotic toxins (VAPs) have been isolated from other snake venoms (Masuda *et al.*, 2001; You *et al.*, 2003; Trummal *et al.*, 2005). VAP1 is a disulfide-bonded homodimeric protein with a molecular weight of 110 kDa and an isoelectric point of 8.5. VAP2 is an acidic single-chain protein with a molecular weight of 55 kDa and an isoelectric point of 4.5 (Masuda *et al.*, 1997, 1998). VAP1 (Masuda *et al.*, 2000) and VAP2 (S. Masuda, H. Hayashi & S. Araki, in preparation) are modular metalloproteinases with nucleotide-sequence homology to genes encoding the mammalian membrane-anchored metalloproteinases known as ADAMs. ADAMs are an emerging class of metalloproteinases whose function has been implicated in cell–cell and cell–matrix adhesion and signalling. They also appear to be associated with numerous diseases including arthritis, Alzheimer's disease and cancer (White, 2003; Blobel, 2005; Seals & Courtneidge, 2003; Moss & Bartsch, 2004; Duffy *et al.*, 2003).

Viperidae snake venoms contain a number of metalloproteinases, the snake-venom metalloproteinases (SVMPs), that induce local and systemic haemorrhage by disrupting the wall of the blood vessels in envenomed patients (Gutierrez *et al.*, 2005). All known VAPs belong to the P-III class of SVMPs, which have been shown to be the most potent haemorrhagic toxins from snake venoms. The P-III SVMPs have a modular structure consisting of metalloproteinase (M), disintegrin (D) and cysteine-rich (C) domains (Fox & Serrano, 2005). SVMPs and ADAMs are members of the reprolysin group of zinc-dependent metalloproteinases, which together with astasins, serralysin and matrix metalloproteinases comprise the metzincin superfamily of metalloproteinases (Bode *et al.*, 1993). All these enzymes share a signature consensus zinc-binding motif, HE*XX*H*XX*G*XX*H, in their catalytic region that defines proteins of the class, as well as a methionine-containing turn that serves as a structural base for the three active histidine residues (Bode *et al.*, 1993).

The crystal structures of several SVMPs of the P-I class, which contain only an M domain, and of isolated domains of ADAMs have

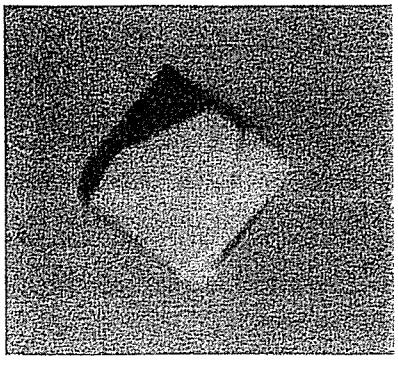

Table 1
Data-collection statistics for VAP1 crystals.

Values in parentheses are for the highest resolution shell. For each data set, a single crystal was used for measurement.

| | Form 1-1 | Form 1-2 |
|---|---|---|
| Space group | $P4_12_12$ | $P2_12_12_1$ |
| Unit-cell parameters | | |
| $a$ (Å) | 93.9 | 86.7 |
| $b$ (Å) | 93.9 | 93.3 |
| $c$ (Å) | 244.8 | 137.7 |
| $\alpha = \beta = \gamma$ (°) | 90 | 90 |
| Beamline (detector) | BL45PX (Rigaku Jupiter) | BL45PX (Rigaku R-AXIS V) |
| Wavelength (Å) | 0.98 | 1.0 |
| Resolution (Å) | 50–2.50 (2.59–2.50) | 50–2.50 (2.59–2.50) |
| No. of unique reflections | 38868 (3773) | 38926 (3800) |
| $R_{merge}$† | 0.084 (0.380) | 0.072 (0.369) |
| $I/\sigma(I)$ | 18.7 (7.1) | 14.4 (2.9) |
| Completeness (%) | 99.7 (99.6) | 99.4 (98.8) |
| Redundancy | 12.7 | 3.91 |
| No. of molecules in ASU | 1 | 1 |
| Matthews value (Å$^3$ Da$^{-1}$) | 2.5 | 2.5 |
| Solvent content (%) | 51 | 51 |

† $R_{merge} = \sum_{hkl}\sum_i |I_i(hkl) - \langle I(hkl)\rangle| / \sum_{hkl}\sum_i I_i(hkl)$, where $I_i(hkl)$ is the $i$th intensity measurement of reflection $hkl$ and $\langle I(hkl)\rangle$ is its average.

been determined. However, structures of SVMPs or ADAMs containing M, D and C domains have not been determined. To understand more about the structure of P-III SVMPs and ADAMs and how it relates to the molecular mechanism of VAP-induced apoptosis, we initiated the crystallographic analysis of VAP1 and VAP2. This is the first report of the crystallization and preliminary X-ray analysis of apoptotic SVMPs. Three-dimensional crystal structures of VAP1 derived from the two distinct crystal forms described in this report have recently been described (Takeda *et al.*, 2006); the structural analysis of VAP2 is ongoing.

## 2. Methods

### 2.1. Purification

VAP1 and VAP2 were purified as described previously (Maruyama *et al.*, 2005; Masuda *et al.*, 1998) with some modifications. Briefly, crude *C. atrox* venom (Sigma–Aldrich, USA) was dissolved in buffer containing 10 m*M* Tris–HCl pH 7.0 and 10 m*M* NaCl and then applied onto a CM-Sepharose (Amersham Bioscience, USA) column equilibrated with the same buffer. VAP2 was eluted from the column with the above buffer, whereas VAP1 was eluted with buffer containing 10 m*M* Tris–HCl pH 7.0 and 50 m*M* NaCl.

The VAP1 was further purified on a hydroxylapatite column. The VAP1-containing CM-Sepharose fraction was first diluted with an equal amount of distilled water and then applied onto a hydroxylapatite column equilibrated with 25 m*M* sodium phosphate pH 7.0. VAP1 was eluted using buffer containing 50 m*M* sodium phosphate pH 7.0 and then concentrated using an Amicon Ultra membrane (Millipore) with a nominal molecular-weight limit (NMWL) of 50 000 Da. The final protein concentration was 6.5 mg ml$^{-1}$. During the concentration step, the buffer was replaced with 10 m*M* Tris–HCl pH 7.0.

The VAP2-containing CM-Sepharose fraction was loaded onto a Resource Q (GM Healthcare) column equilibrated with 10 m*M* Tris–HCl pH 8.0 and 50 m*M* NaCl and then eluted with a gradient of NaCl. 55 kDa molecular-weight fractions, which were eluted at about 130 m*M* NaCl, were pooled and concentrated by Amicon Ultra with a 30 000 NMWL membrane. The final protein concentration was 3.8 mg ml$^{-1}$ in buffer containing 10 m*M* Tris–HCl pH 8.0.

### 2.2. Initial crystallization screen

Initial screening for appropriate crystallization conditions for VAP1 and VAP2 was carried out using the sitting-drop vapour-diffusion method and Crystal Screen (Hampton Research, USA), with or without 63 µg ml$^{-1}$ (almost twice the molar protein concentration) of the hydroxyamate inhibitor 3-(*N*-hydroxycarboxamide)-2-isobutyl-propanoyl-Trp-methylamide (GM6001, Calbiochem) in the protein solution. A volume of 0.3–0.5 µl protein solution was mixed with an equal amount of reservoir solution and droplets were allowed to equilibrate against 0.1 ml reservoir solution at 293 K.

### 2.3. Diffraction data collection

Crystals were cryoprotected, mounted in a nylon loop (Hampton Research, USA) or in a Lytho Loop (Protein Wave Corp., Japan) and immediately exposed to a stream of nitrogen gas at 100 K to flash-freeze the samples. The preliminary X-ray data were collected using an in-house X-ray diffractometer (Rigaku Micromax-007 X-ray generator with R-AXIS VII imaging-plate detector) and crystals that diffracted well were selected for data acquisition using the beamlines at SPring-8. All diffraction data sets were collected using undulator beamlines (BL41XU, BL45XU) at 100 K and diffraction images were processed using the *HKL*2000 software (Otwinowski & Minor, 1997).

## 3. Results

### 3.1. VAP1 crystals

**3.1.1. Crystallization.** VAP1 was reproducibly crystallized in two distinct crystal forms. Crystals were initially obtained using Crystal

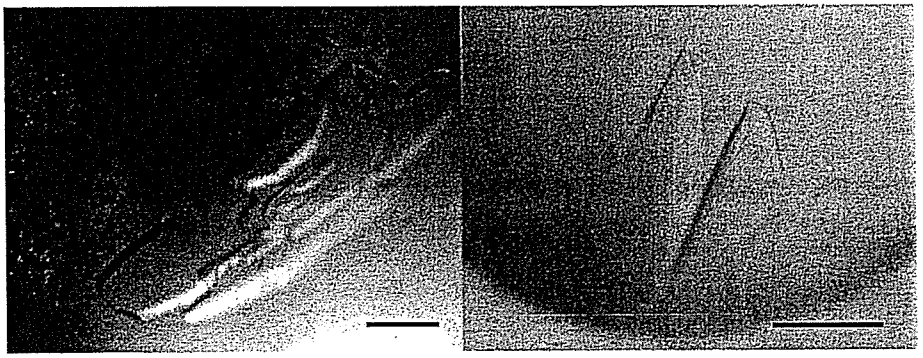

(*a*) (*b*)

Figure 1
VAP1 crystals. (*a*) Form 1-1. (*b*) Form 1-2. The scale bars indicate 0.1 mm.

Table 2
Data-collection statistics for VAP2 crystals.

Values in parentheses are for the highest resolution shell. For each data set, a single crystal was used for measurement.

| | Form 2-1 | Form 2-2 | Form 2-3 | Form 2-4 | Form 2-5 |
|---|---|---|---|---|---|
| GM6001 | + | + | + | + | − |
| Space group | $P2_1$ | $P2_12_12_1$ | $P4_1$ | $P6_522$ | $C2$ |
| Unit-cell parameters | | | | | |
| $a$ (Å) | 56.9 | 57.7 | 60.7 | 156.8 | 220.7 |
| $b$ (Å) | 138.0 | 118.2 | 60.7 | 156.8 | 79.5 |
| $c$ (Å) | 59.2 | 138.5 | 257.9 | 95.6 | 58.7 |
| $\alpha$ (°) | 90 | 90 | 90 | 90 | 90 |
| $\beta$ (°) | 91.5 | 90 | 90 | 90 | 91.7 |
| $\gamma$ (°) | 90 | 90 | 90 | 120 | 90 |
| Beamline (detector) | BL41XU (ADSC Quantum 310R CCD detector) | | | | |
| Wavelength (Å) | 1.0 | 1.0 | 1.0 | 1.0 | 1.0 |
| Resolution (Å) | 50–2.15 (2.23–2.15) | 50–2.50 (2.59–2.50) | 50–3.20 (3.31–3.2) | 50–3.80 (3.94–3.80) | 50–2.70 (2.80–2.70) |
| No. of unique reflections | 48664 (4428) | 33288 (2925) | 15097 (1437) | 7169 (682) | 26911 (2313) |
| $R_{merge}$† | 0.081 (0.196) | 0.089 (0.321) | 0.091 (0.360) | 0.117 (0.397) | 0.085 (0.231) |
| $I/\sigma(I)$ | 9.8 (4.6) | 10.3 (3.7) | 10.9 (4.0) | 8.4 (6.5) | 10.1 (5.5) |
| Completeness (%) | 98.1 (89.5) | 98.6 (88.4) | 99.5 (95.7) | 99.8 (99.9) | 95.9 (82.5) |
| Redundancy | 3.3 | 6.5 | 7.0 | 19.2 | 3.4 |
| No. of molecules in ASU | 2 | 2 | 2 | 1 | 2 |
| Matthews value (Å$^3$ Da$^{-1}$) | 2.4 | 2.4 | 2.5 | 3.1 | 2.7 |
| Solvent content (%) | 49 | 49 | 50 | 60 | 54 |

† $R_{merge} = \sum_{hkl}\sum_i |I_i(hkl) - \langle I(hkl)\rangle| / \sum_{hkl}\sum_i I_i(hkl)$, where $I_i(hkl)$ is the $i$th intensity measurement of reflection $hkl$ and $\langle I(hkl)\rangle$ is its average.

Screen solution No. 46, but these crystals diffracted poorly. Subsequently, droplets were prepared by mixing 1 µl protein solution and 1 µl reservoir solution containing 15% PEG 8000, 0.1 *M* sodium cacodylate pH 6.5 and then equilibrated against 1 ml reservoir solution. Within a couple of weeks, using the hanging-drop method, improved tetragonal crystals (form 1-1; Fig. 1*a*) were obtained.

Orthorhombic crystals (form 1-2; Fig. 1*b*) were obtained using Additive Screen (Hampton Research, USA). The droplet was made by mixing 0.3 µl protein solution and 0.3 µl reservoir solution supplemented with one-fifth of the volume of 0.1 *M* cobalt(II) chloride (Additive Screen solution No. 4). The best crystals were obtained using the sitting-drop method after equilibration for 3 d against 0.1 ml of the same reservoir solution used to obtain form 1-1 crystals.

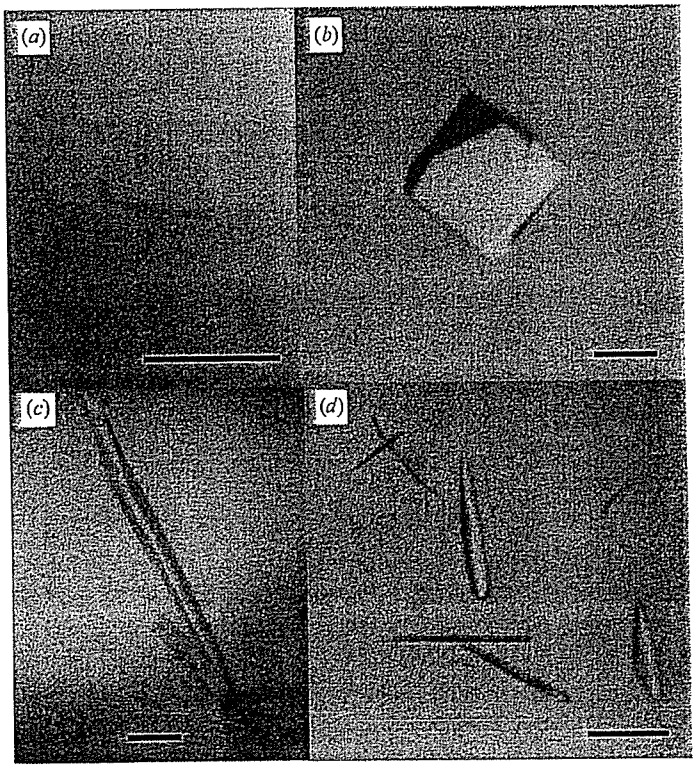


**Figure 2**
VAP2 crystals. (*a*) Form 2-2, (*b*) form 2-3, (*c*) form 2-4 and (*d*) form 2-5 crystals. The scale bars indicate 0.1 mm.

**3.1.2. X-ray analysis.** For X-ray measurements, crystals of either crystal form were soaked in a solution containing 15% PEG 8000, 5% methanol, 20% xylitol and 0.1 *M* sodium cacodylate pH 6.5 for cryoprotection prior to flash-freezing. X-ray diffraction data were obtained by the oscillation method using beamline BL45XU and an oscillation angle of 0.75° per image. Data sets were collected using a CCD detector (Rigaku Jupiter) for crystal form 1-1 or an imaging-plate detector (Rigaku R-AXIS V) for crystal form 1-2. The unit-cell parameters and the data statistics for the two crystal forms are summarized in Table 1. The structures were determined at 2.5 Å resolution by the molecular-replacement method using the P-I SVMP acutolysin-C (PDB code 1qua) as a starting model (Takeda *et al.*, 2006). The coordinates and the structure factors have been deposited in the PDB (2erq for form 1-1 and 2ero for form 1-2 crystals).

### 3.2. VAP2 crystals

**3.2.1. Crystallization.** Five distinct crystal forms of VAP2 were analyzed by X-ray diffraction. The initial screening for VAP2 crystals was performed in the presence and absence of the inhibitor GM6001.

In the presence of GM6001, Crystal Screen solution No. 10 yielded crystals. With this as a starting condition, the pH of the mother liquor, the PEG concentration and molecular weight and the species and concentrations of salts and additives were optimized and four distinct crystal forms were obtained (forms 2-1, 2-2, 2-3 and 2-4). These four forms were only obtained in the presence of GM6001 and were never obtained in its absence. Monoclinic (form 2-1) and orthorhombic (form 2-2; Fig. 2*a*) forms were obtained by the sitting-drop method under identical conditions as follows: droplets were made by mixing 0.5 µl protein solution with 0.5 µl reservoir solution containing 30% PEG 8000, 0.1 *M* ammonium acetate, 0.1 *M* sodium cacodylate pH 6.5 and were equilibrated against 0.1 ml reservoir solution. Tetragonal form crystals (form 2-3; Fig. 2*b*) were obtained by adding a one-tenth volume of 1 *M* potassium chloride (Additive Screen solution No. 16)

to the mother liquor and using a reservoir solution containing 30% PEG 8000, 0.1 *M* ammonium acetate, 0.1 *M* sodium acetate pH 4.6 with the same drop and reservoir volumes described above. Hexagonal crystals (form 2-4; Fig. 2*c*) were obtained by the hanging-drop method using 1 ml of a reservoir solution containing 20% PEG 20 000, 0.2 *M* calcium acetate, 0.1 *M* sodium cacodylate pH 6.5. The droplet was made by mixing 1 µl protein solution and 1 µl reservoir solution supplemented with a one-fifth volume of 0.3 *M* glycyl-glycyl-glycine solution (Additive Screen solution No. 34).

In the absence of GM6001, crystals were obtained with Crystal Screen solution No. 46, but these crystals yielded poor diffraction data. To improve the quality of the crystals, several additives were screened. Monoclinic crystals (form 2-5; Fig. 2*d*) were obtained by adding a one-tenth volume of 40% *n*-propanol solution (Additive Screen solution No. 90) to the reservoir solution (final composition 4% *n*-propanol, 16.2% PEG 8000, 0.18 *M* calcium acetate, 0.09 *M* sodium cacodylate pH 6.5). A mixture of 0.5 µl protein solution and 0.5 µl reservoir solution was equilibrated against 0.1 ml reservoir solution. These form 2-5 crystals were only obtained in the absence of GM6001 and were never obtained in its presence.

**3.2.2. X-ray analysis.** The mother liquors of the form 2-2 and 2-3 crystals were suitable for freezing; all others were first cryoprotected. For form 2-1 and 2-4 crystals, 20% glycerol was added to the reservoir solution for cryoprotection. For form 2-1, the cryogenic solution was added gradually to the crystal droplet in order to avoid cracking induced by osmotic shock. Crystal form 2-5 was rinsed in a solution containing 15% PEG 8000, 5% methanol, 20% xylitol and 0.1 *M* sodium cacodylate pH 6.5 and then immediately flash-frozen at 100 K. Because these crystals were extremely thin and fragile, they were mounted in a LithoLoop, an etched Mylar film, to prevent bending of the crystal.

All diffraction data sets for the VAP2 crystals were acquired using the oscillation method and beamline BL41XU (the oscillation angle was 1.0° for all data sets) at a wavelength of 1.0 Å and data were collected using an ADSC Quantum 310R detector. The unit-cell parameters and statistics for the data sets are summarized in Table 2. The estimated number of molecules in the asymmetric unit for each crystal form was obtained by a preliminary molecular-replacement method using *MOLREP* from the *CCP*4 suite (Collaborative Computational Project, Number 4, 1994) and the metalloproteinase (M) and cysteine-rich (C) domains of VAP1 (Takeda *et al.*, 2006) as the starting models. Structural analyses of these crystals along with the molecular-replacement phases are ongoing.

We thank Mariko Tomisako for her help in crystallization experiments and the staff of SPring-8 for assistance with data acquisition. This work was partly supported by Grant Nano-001 for Research on Advanced Medical Technology from the Ministry of Health, Labour and Welfare of Japan and by grants from the Takeda Science Foundation, from the Kao Foundation for Arts and Science and from the Senri Life Science Foundation.

## References

Araki, S., Ishida, T., Yamamoto, T., Kaji, K. & Hayashi, H. (1993). *Biochem. Biophys. Res. Commun.* **190**, 148–153.
Blobel, C. P. (2005). *Nature Rev. Mol. Cell Biol.* **6**, 32–43.
Bode, W., Gomis-Ruth, F. X. & Stockler, W. (1993). *FEBS Lett.* **331**, 134–140.
Collaborative Computational Project, Number 4 (1994). *Acta Cryst.* D**50**, 760–763.
Duffy, M. J., Lynn, D. J., Lloyd, A. T. & O'Shea, C. M. (2003). *Thromb. Haemost.* **89**, 622–631.
Fox, J. W. & Serrano, S. M. (2005). *Toxicon*, **45**, 969–985.
Gutierrez, J. M., Rucavado, A., Escalante, T. & Diaz, C. (2005). *Toxicon*, **45**, 997–1011.
Maruyama, J., Hayashi, H., Miao, J., Sawada, H. & Araki, S. (2005). *Toxicon*, **46**, 1–6.
Masuda, S., Araki, S., Yamamoto, T., Kaji, K. & Hayashi, H. (1997). *Biochem. Biophys. Res. Commun.* **235**, 59–63.
Masuda, S., Hayashi, H. & Araki, S. (1998). *Eur. J. Biochem.* **253**, 36–41.
Masuda, S., Hayashi, H., Atoda, H., Morita, T. & Araki, S. (2001). *Eur. J. Biochem.* **268**, 3339–3345.
Masuda, S., Ohta, T., Kaji, K., Fox, J. W., Hayashi, H. & Araki, S. (2000). *Biochem. Biophys. Res. Commun.* **278**, 197–204.
Moss, M. L. & Bartsch, J. W. (2004). *Biochemistry*, **43**, 7227–7235.
Otwinowski, Z. & Minor, W. (1997). *Methods Enzymol.* **276**, 307–326.
Seals, D. F. & Courtneidge, S. A. (2003). *Genes Dev.* **17**, 7–30.
Takeda, S., Igarashi, T., Mori, H. & Araki, S. (2006). *EMBO J.* **25**, 2388–2396.
Trummal, K., Tonismagi, K., Siigur, E., Aaspollu, A., Lopp, A., Sillat, T., Saat, R., Kasak, L., Tammiste, I., Kogerman, P., Kalkkinen, N. & Siigur, J. (2005). *Toxicon*, **46**, 46–61.
White, J. M. (2003). *Curr. Opin. Cell Biol.* **15**, 598–606.
You, W. K., Seo, H. J., Chung, K. H. & Kim, D. S. (2003). *J. Biochem. (Tokyo)*, **134**, 739–749.

Available online at www.sciencedirect.com
ScienceDirect
Radiation Physics and Chemistry 75 (2006) 1841–1849
Radiation Physics and Chemistry
www.elsevier.com/locate/radphyschem

# K-edge angiography utilizing a tungsten plasma X-ray generator in conjunction with gadolinium-based contrast media

Eiichi Sato[a,*], Yasuomi Hayasi[a], Etsuro Tanaka[b], Hidezo Mori[c], Toshiaki Kawai[d], Takashi Inoue[e], Akira Ogawa[e], Shigehiro Sato[f], Kazuyoshi Takayama[g], Jun Onagawa[h], Hideaki Ido[h]

[a]*Department of Physics, Iwate Medical University, 3-16-1 Honchodori, Morioka 020-0015, Japan*
[b]*Department of Nutritional Science, Faculty of Applied Bio-science, Tokyo University of Agriculture, 1-1-1 Sakuragaoka, Setagaya-ku 156-8502, Japan*
[c]*Department of Cardiac Physiology, National Cardiovascular Center Research Institute, 5-7-1 Fujishirodai, Suita, Osaka 565-8565, Japan*
[d]*Electron Tube Division #2, Hamamatsu Photonics K. K., 314-5 Shimokanzo, Iwata 438-0193, Japan*
[e]*Department of Neurosurgery, School of Medicine, Iwate Medical Universichimaru, Morioka 020-8505, Japan*
[f]*Department of Microbiology, School of Medicine, Iwate Medical University, 19-1 Uchimaru, Morioka 020-8505, Japan*
[g]*Shock Wave Research Center, Institute of Fluid Science, Tohoku University, 2-1-1 Katahira, Sendai 980-8577, Japan*
[h]*Department of Applied Physics and Informatics, Faculty of Engineering, Tohoku Gakuin University, 1-13-1 Chuo, Tagajo 985-8537, Japan*

Accepted 23 November 2005

**Abstract**

The tungsten plasma flash X-ray generator is useful in order to perform high-speed enhanced K-edge angiography using cone beams because K-series characteristic X-rays from the tungsten target are absorbed effectively by gadolinium-based contrast media. In the flash X-ray generator, a 150 nF condenser is charged up to 80 kV by a power supply, and flash X-rays are produced by the discharging. The X-ray tube is a demountable diode, and the turbomolecular pump evacuates air from the tube with a pressure of approximately 1 mPa. Since the electric circuit of the high-voltage pulse generator employs a cable transmission line, the high-voltage pulse generator produces twice the potential of the condenser charging voltage. At a charging voltage of 80 kV, the estimated maximum tube voltage and current were approximately 160 kV and 40 kA, respectively. When the charging voltage was increased, the characteristic X-ray intensities of tungsten $K_\alpha$ lines increased. The $K_\alpha$ lines were clean, and hardly any bremsstrahlung rays were detected. The X-ray pulse widths were approximately 110 ns, and the time-integrated X-ray intensity had a value of approximately 0.35 mGy at 1.0 m from the X-ray source with a charging voltage of 80 kV. Angiography was performed

*Corresponding author.
*E-mail address:* dresato@iwate-med.ac.jp (E. Sato).

0969-806X/$ - see front matter 
doi:10.1016/j.radphyschem.2005.11.015

using a film-less computed radiography (CR) system and gadolinium-based contrast media. In angiography of non-living animals, we observed fine blood vessels of approximately 100 μm with high contrasts.


*PACS:* 52.59.Mv; 52.80.Vp; 87.59.Dj; 87.64.Gb

*Keywords:* Angiography; Gadolinium-based contrast media; Characteristic X-rays; Quasi-monochromatic X-rays; Tungsten $K_\alpha$ lines

## 1. Introduction

The successful uses of monochromatic parallel beams from synchrotron orbital radiation in recent years have greatly increased the demand for phase-contrast radiography (Davis et al., 1995; Momose et al., 1996; Ando et al., 2002) and enhanced K-edge angiography (Thompson et al., 1992; Mori et al., 1996; Hyodo et al., 1998). In particular, the parallel beams with photon energies of approximately 35 keV have been employed to perform angiography, because the beams are absorbed effectively by iodine-based contrast media with a K-absorption edge of 33.2 keV. Without using a synchrotron, we have developed an X-ray generator utilizing a cerium-target tube, and have performed cone-beam K-edge angiography achieved with cerium $K_\alpha$ rays of 34.6 keV (Sato et al., 2004a, b, c).

Gadolinium-based contrast media with a K-edge of 50.2 keV have been employed to perform magnetic resonance angiography (MRA), and the gadolinium density has been increasing. In view of this situation, ytterbium $K_\alpha$ rays (52.0 keV) are useful for enhanced K-edge angiography, because the $K_\alpha$ rays are absorbed effectively by gadolinium media. As compared with angiography using iodine media, the absorbed dose can be decreased considerably utilizing angiography achieved with gadolinium media. However, because ytterbium is a lanthanide series element and tends to oxidize in the atmosphere, $K_\alpha$ rays of tantalum (57.1 keV) and tungsten (58.9 keV) are also useful to perform angiography.

To produce high-dose-rate X-rays, several different flash X-ray generators have been developed (Sato et al., 1990, 1994a, b; Shikoda et al., 1994; Takahashi et al., 1994), and plasma flash X-ray generators (Sato et al., 2003a, b, 2004a, b, c, 2005a, b, c) have been developed to perform a preliminary experiment for producing hard X-ray lasers. In the plasma, the bremsstrahlung X-rays are absorbed effectively and are converted into fluorescent rays, and intense and clean K-series characteristic X-rays of nickel and copper have been produced from the axial direction of weakly ionized linear plasma. However, it is difficult to increase the photon energies of characteristic X-rays because the plasma transmits high-photon-energy bremsstrahlung X-rays. In view of this situation, we have developed a compact flash X-ray generator (Sato et al., 2004a, b, c, 2005a, b, c) and have succeeded in producing clean high-photon-energy characteristic X-rays utilizing the angle dependence of bremsstrahlung X-rays, because bremsstrahlung rays are not emitted in the opposite direction to that of electron trajectory in Sommerfeld's theory.

In this article, we describe an intense quasi-monochromatic plasma flash X-ray generator with a tungsten target tube, and used it to perform a preliminary study on angiography achieved with tungsten $K_\alpha$ rays.

## 2. Principle of K-edge angiography

Fig. 1 shows the mass attenuation coefficients of gadolinium at the selected energies; the coefficient curve is discontinuous at the gadolinium K-edge. The average photon energy of the tungsten $K_\alpha$ lines is shown above the gadolinium K-edge. The average photon energy is 58.9 keV, and gadolinium contrast media with a K-absorption edge of 50.2 keV absorb the lines easily. Therefore, blood vessels were observed with high contrasts.

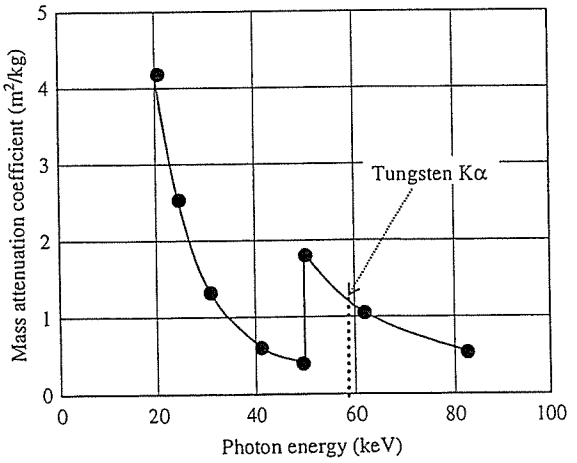


Fig. 1. Mass attenuation coefficients of gadolinium. The average photon energy of tungsten $K_\alpha$ lines is shown above gadolinium K edge.

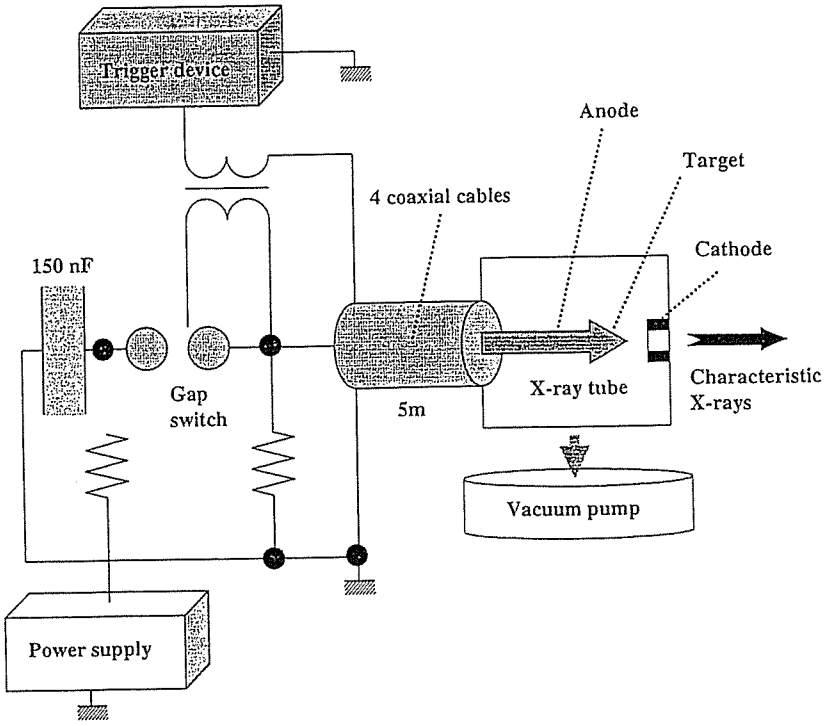


Fig. 2. Block diagram including the high-voltage circuit of the intense quasi-monochromatic plasma flash X-ray generator with a tungsten-target tube.

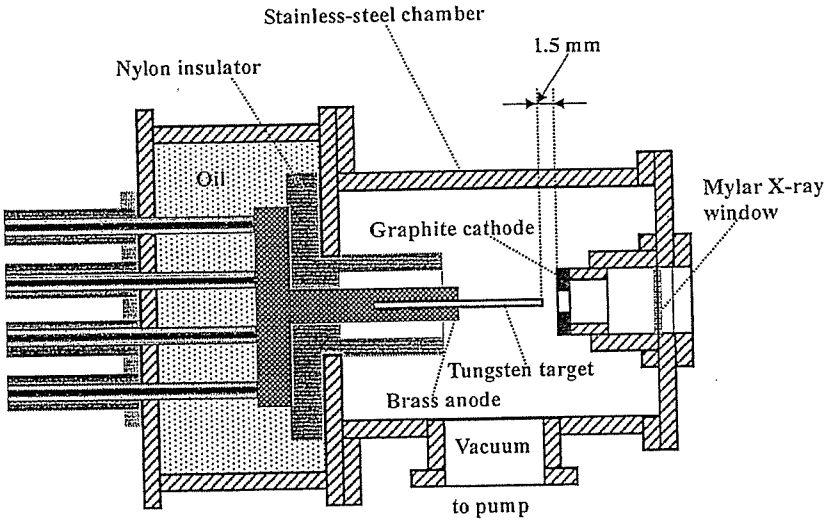


Fig. 3. Schematic drawing of a flash X-ray tube with a rod-shaped tungsten target.

## 3. Generator

### 3.1. High-voltage circuit

Fig. 2 shows a block diagram of a high-intensity plasma flash X-ray generator. The generator consists of the following essential components: a high-voltage power supply, a high-voltage condenser with a capacity of approximately 150 nF, an air gap switch, a turbomolecular pump, a thyratron pulse generator as a trigger device and a flash X-ray tube. In this generator, a coaxial cable transmission line is employed in order to

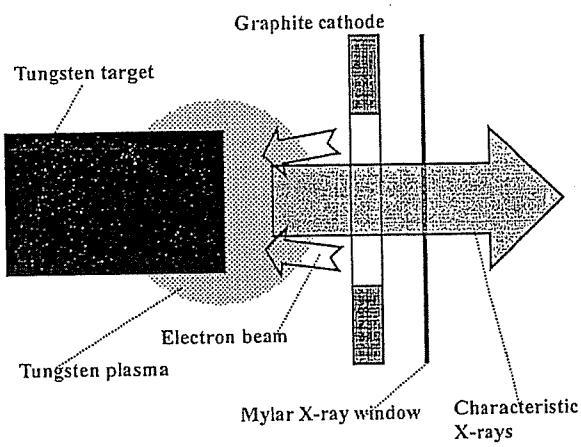


Fig. 4. Irradiation of K-series characteristic X-rays of tungsten.

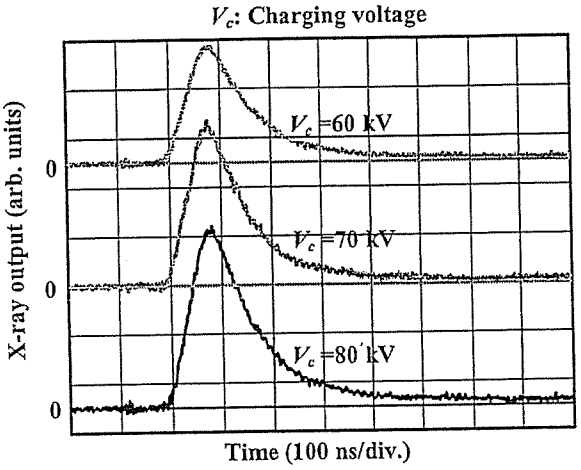


Fig. 5. X-ray outputs detected using a combination of a plastic scintillator and a photomultiplier.

increase maximum tube voltage using high-voltage reflection. The high-voltage main condenser is charged up to 80 kV by the power supply, and electric charges in the condenser are discharged to the tube through the four cables after closing the gap switch with the trigger device.

### 3.2. X-ray tube

The X-ray tube is a demountable cold-cathode diode that is connected to the turbomolecular pump with a pressure of approximately 1 mPa (Fig. 3). This tube consists of the following major parts: a ring-shaped graphite cathode with an inside diameter of 4.5 mm, a stainless-steel vacuum chamber, a nylon insulator, a polyethylene terephthalate (Mylar) X-ray window 0.25 mm in thickness and a rod-shaped tungsten target 3.0 mm in diameter. The distance between the target and cathode electrodes can be regulated from the outside of the tube, and is set to 1.5 mm. As electron beams from the cathode electrode are roughly converged to the target by the electric field in the tube, evaporation leads to the formation of weakly ionized plasma, consisting of tungsten ions and electrons, around the target. Because bremsstrahlung rays are not emitted in the opposite direction to that of electron trajectory (Fig. 4), tungsten K-series characteristic X-rays can be produced without using a filter.

## 4. Characteristics

### 4.1. Tube voltage and current

In this generator, it was difficult to measure the tube voltage and current since the tube voltages were high, and there was no space to set a current transformer for measuring the tube current. Currently, the voltage and

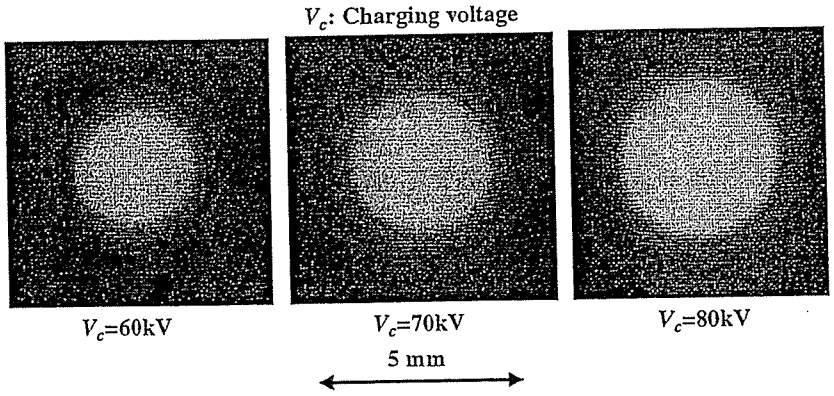


Fig. 6. Images of characteristic X-ray source obtained using a pinhole camera with changes in the charging voltage.

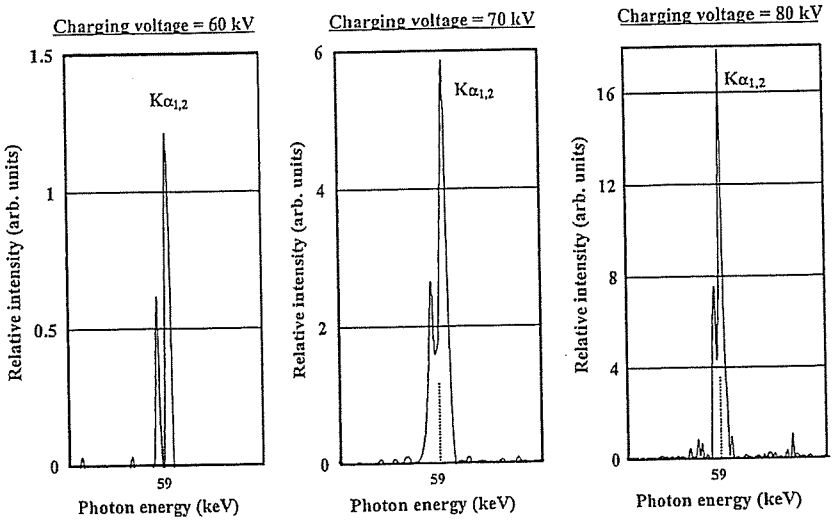


Fig. 7. X-ray spectra from a tungsten target. The spectra were measured using a transmission type spectrometer with a lithium fluoride curved crystal.

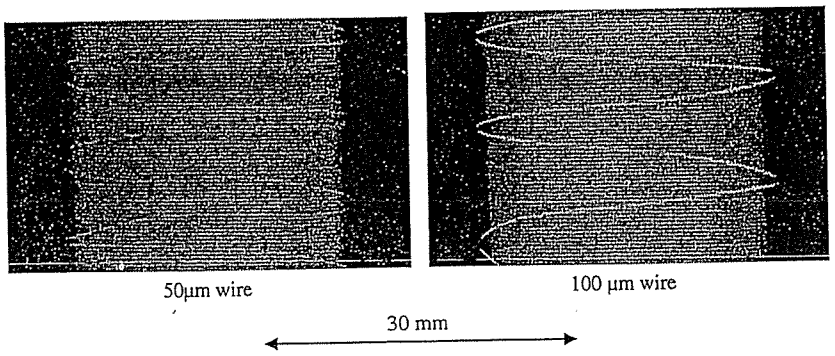


Fig. 8. Radiograms of tungsten wires coiled around rods made of polymethyl methacrylate.

current roughly display damped oscillations. When the charging voltage was increased, both the maximum tube voltage and current increased. At a charging voltage of 80 kV, the estimated maximum values of the tube voltage and current were approximately 160 kV (two times the charging voltage) and 40 kA, respectively.

### 4.2. X-ray output

X-ray output pulse was detected using a combination of a plastic scintillator and a photomultiplier (Fig. 5). The X-ray pulse height substantially increased with corresponding increases in the charging voltage. The X-ray pulse widths were approximately 110 ns, and the time-integrated X-ray intensity measured by a thermoluminescence dosimeter (Kyokko TLD Reader 1500 having MSO-S elements without energy compensation) had a value of approximately 0.35 mGy at 1.0 m from the X-ray source with a charging voltage of 80 kV.

### 4.3. X-ray source

In order to observe the plasma X-ray source, we employed a 100-μm-diameter pinhole camera and an X-ray film (Polaroid XR-7) (Fig. 6). When the charging voltage was increased, the plasma X-ray source grew, and both spot dimension and intensity increased. Because the X-ray intensity is the highest at the center of the spot, both the dimension and intensity decreased according to both increases in the thickness of a filter for absorbing X-rays and decreases in the pinhole diameter.

### 4.4. X-ray spectra

X-ray spectra were measured using a transmission-type spectrometer with a lithium fluoride curved crystal 0.5 mm in thickness. The X-ray intensities of the spectra were detected by an imaging plate of a computed radiography (CR) system (Sato et al., 2000) (Konica Minolta Regius 150) with a wide dynamic range, and

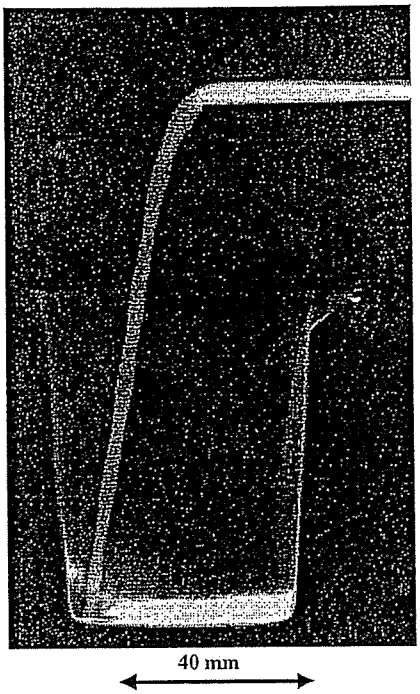


Fig. 9. Radiogram of water falling into polypropylene beaker from a glass test tube.

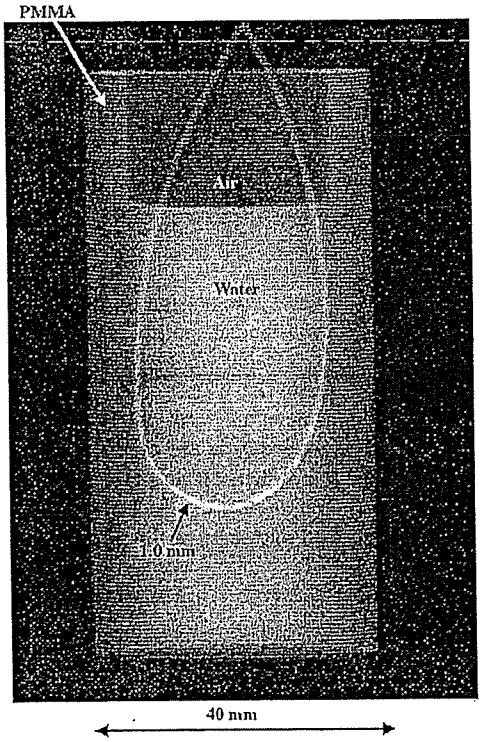


Fig. 10. Angiography of a Teflon tube using a contrast medium which contains approximately 65% gadodiamidehydrate.

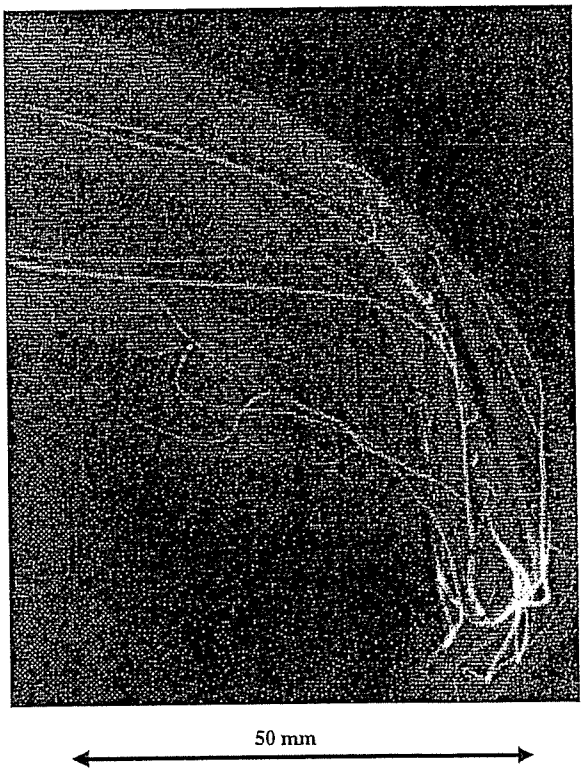


Fig. 11. Angiography of a rabbit ear using gadolinium oxide powder.

relative X-ray intensity was calculated from Dicom original digital data corresponding to X-ray intensity; the data was scanned by Dicom viewer in the film-less CR system. Subsequently, the relative X-ray intensity as a function of the data was calibrated using a conventional X-ray generator, and we confirmed that the intensity was proportional to the exposure time. Fig. 7 shows measured spectra from the tungsten target. We observed clean $K_\alpha$ lines, while bremsstrahlung rays were hardly detected. The $K_\alpha$ intensity substantially increased with increases in the charging voltage.

## 5. Angiography

The flash angiography was performed by the CR system at 1.2 m from the X-ray source, and the charging voltage was 80 kV.

Firstly, rough measurements of spatial resolution were made using wires. Fig. 8 shows radiograms of tungsten wires coiled around rods made of polymethyl methacrylate (PMMA). Although the image contrast decreased somewhat with decreases in the wire diameter, due to blurring of the image caused by the sampling pitch of 87.5 μm, a 50-μm-diameter wire could be observed.

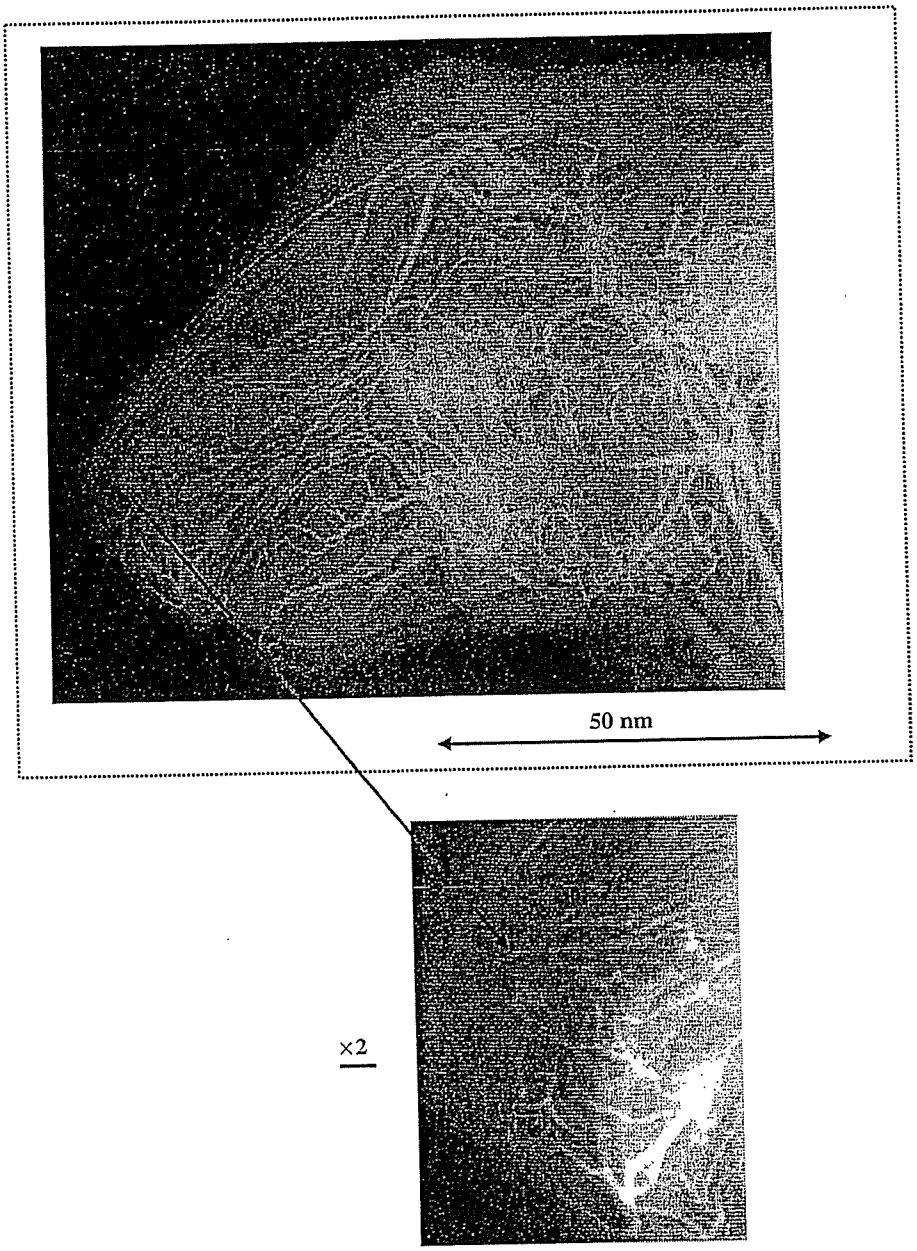


Fig. 12. Angiography of a rabbit head using gadolinium oxide powder.

The image of water (20% gadolinium oxide suspension) falling into a polypropylene beaker from a plastic test tube is shown in Fig. 9. The diameter of gadolinium oxide powder ranges from 1 to 10 μm. Because the X-ray duration was about 100 ns, the stop-motion image of water could be obtained.

Fig. 10 shows an angiogram of a polytetrafluoroethylene (Teflon) tube in a PMMA case using a contrast medium which contains approximately 65% gadodiamidehydrate, and a high-contrast tube with a bore diameter of 1.0 mm is observed. Figs. 11 and 12 show angiograms of a rabbit ear and head using gadolinium oxide powder, and fine blood vessels of approximately 100 μm were visible.

## 6. Conclusions and outlook

In summary, we succeeded in producing $K_\alpha$ rays of tungsten and in performing K-edge angiography using gadolinium contrast media with a K-edge of 50.2 keV, and this K-edge angiography could be a useful technique

to decrease the dose absorbed by patients. Although we employed tungsten $K_\alpha$ (58.9 keV) rays, L-series characteristic rays should be absorbed before angiography using a filter.

We obtained sufficient X-ray intensity for CR angiography with X-ray durations of approximately 100 ns, and the intensity can be increased by increasing the charging voltage at a constant target–cathode space. In an empirical equation, because the characteristic X-ray intensity is proportional to approximately 1.5th power of the voltage difference between the tube voltage and the critical excitation voltage, optimum intensity for angiography can be controlled. In this research, the generator produced instantaneous number of K photons was approximately $1 \times 10^9$ photons/cm$^2$ per pulse at 1.0 m from the source.

Because the dimensions of the X-ray source are primarily determined by the target diameter, the diameter should be minimized in order to improve the spatial resolution, and can be reduced to approximately 0.5 mm. Subsequently, the sampling pitch can be decreased to 43.8 μm using a CR system (Konica Minolta Regius 190) to observe fine blood vessels of approximately 50 μm diameter.

Using this flash X-ray generator, enhanced K-edge angiography using iodine contrast media can also be performed using a cerium target. In addition, steady-state monochromatic X-rays can be produced by a similar tube utilizing a hot cathode and a constant high-voltage power supply. In addition, fine focusing can be realized using tungsten or molybdenum target, and these X-ray generators could be employed to perform quasi-monochromatic phase-contrast radiography for edge enhancement.

## Acknowledgments

This work was supported by Grants-in-Aid for Scientific Research (13470154, 13877114, 16591181 and 16591222) and Advanced Medical Scientific Research from MECSST, Health and Labor Sciences Research Grants (RAMT-nano-001, RHGTEFB-genome-005 and RHGTEFB-saisei-003), grants from the Keiryo Research Foundation, the Promotion and Mutual Aid Corporation for Private Schools of Japan, the Japan Science and Technology Agency (JST) and the New Energy and Industrial Technology Development Organization (NEDO, Industrial Technology Research Grant Program in 2003).

## References

Ando, M., Maksimenko, M., Sugiyama, H., Pattanasiriwisawa, W., Hyodo, K., Uyama, C., 2002. A simple X-ray dark- and bright-field imaging using achromatic Laue optics. Jpn. J. Appl. Phys. 41, L1016–L1018.

Davis, T.J., Gao, D., Gureyev, T.E., Stevenson, A.W., Wilkins, S.W., 1995. Phase-contrast imaging of weakly absorbing materials using hard X-rays. Nature 373, 595–597.

Hyodo, K., Ando, M., Oku, Y., Yamamoto, S., Takeda, T., Itai, Y., Ohtsuka, S., Sugishita, Y., Tada, J., 1998. Development of a two-dimensional imaging system for clinical applications of intravenous coronary angiography using intense synchrotron radiation produced by a multipole wiggler. J. Synchrotron Rad. 5, 1123–1126.

Momose, A., Takeda, T., Itai, Y., Hirano, K., 1996. Phase-contrast X-ray computed tomography for observing biological soft tissues. Nat. Med. 2, 473–475.

Mori, H., Hyodo, K., Tanaka, E., Mohammed, M.U., Yamakawa, A., Shinozaki, Y., Nakazawa, H., Tanaka, Y., Sekka, T., Iwata, Y., Honda, S., Umetani, K., Ueki, H., Yokoyama, T., Tanioka, K., Kubota, M., Hosaka, H., Ishizawa, N., Ando, M., 1996. Small-vessel radiography in situ with monochromatic synchrotron radiation. Radiology 201, 173–177.

Sato, E., Kimura, S., Kawasaki, S., Isobe, H., Takahashi, K., Tamakawa, Y., Yanagisawa, T., 1990. Repetitive flash X-ray generator utilizing a simple diode with a new type of energy-selective function. Rev. Sci. Instrum. 61, 2343–2348.

Sato, E., Takahashi, K., Sagae, M., Kimura, S., Oizumi, T., Hayasi, Y., Tamakawa, Y., Yanagisawa, T., 1994a. Sub-kilohertz flash X-ray generator utilizing a glass-enclosed cold-cathode triode. Med. Biol. Eng. Comput. 32, 289–294.

Sato, E., Sagae, M., Takahashi, K., Shikoda, A., Oizumi, T., Hayasi, Y., Tamakawa, Y., Yanagisawa, T., 1994b. 10kHz microsecond pulsed X-ray generator utilizing a hot-cathode triode with variable durations for biomedical radiography. Med. Biol. Eng. Comput. 32, 295–301.

Sato, E., Sato, K., Tamakawa, Y., 2000. Film-less computed radiography system for high-speed imaging. Ann. Rep. Iwate Med. Univ. Sch. Lib. Arts Sci. 35, 13–23.

Sato, E., Hayasi, Y., Germer, R., Tanaka, E., Mori, H., Kawai, T., Obara, H., Ichimaru, T., Takayama, K., Ido, H., 2003a. Irradiation of intense characteristic X-rays from weakly ionized linear molybdenum plasma. Jpn. J. Med. Phys. 23, 123–131.

Sato, E., Hayasi, Y., Germer, R., Tanaka, E., Mori, H., Kawai, T., Ichimaru, T., Takayama, K., Ido, H., 2003b. Quasi-monochromatic flash X-ray generator utilizing weakly ionized linear copper plasma. Rev. Sci. Instrum. 74, 5236–5240.

Sato, E., Sagae, M., Tanaka, E., Hayasi, Y., Germer, R., Mori, H., Kawai, T., Ichimaru, T., Sato, S., Takayama, Y., Ido, H., 2004a. Quasi-monochromatic flash X-ray generator utilizing a disk-cathode molybdenum tube. Jpn. J. Appl. Phys. 43, 7324–7328.

Sato, E., Hayasi, Y., Germer, R., Tanaka, E., Mori, H., Kawai, T., Ichimaru, T., Sato, S., Takayama, K., Ido, H., 2004b. Sharp characteristic X-ray irradiation from weakly ionized linear plasma. J. Electron Spectrosc. Related Phenom. 137–140, 713–720.

Sato, E., Tanaka, E., Mori, H., Kawai, T., Ichimaru, T., Sato, S., Takayama, K., Ido, H., 2004c. Demonstration of

enhanced K-edge angiography using a cerium target X-ray generator. Med. Phys. 31, 3017–3021.

Sato, E., Tanaka, E., Mori, H., Kawai, T., Ichimaru, T., Sato, S., Takayama, Y., Ido, H., 2005a. Compact monochromatic flash X-ray generator utilizing a disk-cathode molybdenum tube. Med. Phys. 32, 49–54.

Sato, E., Tanaka, E., Mori, H., Kawai, T., Sato, S., Takayama, Y., 2005b. High-speed enhanced K-edge angiography utilizing cerium plasma X-ray generator. Opt. Eng. 44, 049001–049016.

Sato, E., Tanaka, E., Mori, H., Kawai, T., Sato, S., Takayama, Y., 2005c. Clean monochromatic X-ray irradiation from weakly ionized linear copper plasma. Opt. Eng. 44, 049002–049016.

Shikoda, A., Sato, E., Sagae, M., Oizumi, T., Tamakawa, Y., Yanagisawa, T., 1994. Repetitive flash X-ray generator having a high-durability diode driven by a two-cable-type line pulser. Rev. Sci. Instrum. 65, 850–856.

Takahashi, K., Sato, E., Sagae, M., Oizumi, T., Tamakawa, Y., Yanagisawa, T., 1994. Fundamental study on a long-duration flash X-ray generator with a surface-discharge triode. Jpn. J. Appl. Phys. 33, 4146–4151.

Thompson, A.C., Zeman, H.D., Brown, G.S., Morrison, J., Reiser, P., Padmanabahn, V., Ong, L., Green, S., Giacomini, J., Gordon, H., Rubenstein, E., 1992. First operation of the medical research facility at the NSLS for coronary angiography. Rev. Sci. Instrum. 63, 625–628.

ELSEVIER

Cardiovascular Research 72 (2006) 412–421

Cardiovascular Research

www.elsevier.com/locate/cardiores

# Heavy ion radiation up-regulates Cx43 and ameliorates arrhythmogenic substrates in hearts after myocardial infarction

Mari Amino [a,f,1], Koichiro Yoshioka [a,1], Teruhisa Tanabe [a], Etsuro Tanaka [b], Hidezo Mori [c], Yoshiya Furusawa [d], Wojciech Zareba [e], Masatoshi Yamazaki [f], Harumichi Nakagawa [f], Haruo Honjo [f], Kenji Yasui [f], Kaichiro Kamiya [f], Itsuo Kodama [f,*]

[a] *Department of Cardiology, Tokai University School of Medicine, Isehara, Japan*
[b] *Department of Nutritional Sciences, Tokyo University of Agriculture, Tokyo, Japan*
[c] *Department of Cardiac Physiology, National Cardiovascular Center Research Institute, Osaka, Japan*
[d] *National Institute of Radiological Sciences, Chiba, Japan*
[e] *Cardiology Unit, University of Rochester, Rochester, USA*
[f] *Research Institute of Environmental Medicine, Nagoya University, Nagoya, Japan*

Received 4 June 2006; received in revised form 12 September 2006; accepted 15 September 2006
Available online 20 September 2006
**Time for primary review 17 days**

**Abstract**

**Objective:** Radiation has been shown to enhance intercellular communication in the skin and lungs through an increase of connexin43 (Cx43) expression. If analogous Cx43 up-regulation is induced in the diseased heart, it would provide a new perspective in radiation therapy for arrhythmias. The aim of the present study is to test this hypothesis.
**Methods:** Non-transmural myocardial infarction (MI) was created in 24 rabbits by microsphere injection into the coronary arteries. Twenty-four rabbits without MI were used as controls. Targeted external heavy ion beam irradiation (THIR; 15 Gy) was applied 2 weeks after MI with an accelerator (HIMAC, Chiba, Japan).
**Results:** The THIR was associated with an increase of Cx43 mRNA and protein levels in the left ventricle in control as well as in MI rabbits. THIR also increased lateralization of Cx43, which was no longer colocalized with cadherins. In MI hearts, immunoreactive Cx43 signals were reduced in the peri-infarct zone, and the reduction was reversed by THIR. *In-vivo* epicardial potential mapping on the free wall (64 unipolar electrodes to cover 7×7 mm) in MI hearts revealed reduced conduction velocity, whereas dispersion of the activation-recovery interval (ARI) was increased compared with controls, and these changes were reversed by THIR. The vulnerability for ventricular tachyarrhythmias (VT/VF), which was estimated by programmed stimulation, was increased in MI hearts, and this increased vulnerability to arrhythmias was reversed by THIR.
**Conclusions:** THIR increases Cx43 expression, improves the conductivity, decreases the spatial heterogeneity of repolarization, and reduces the vulnerability of rabbit hearts to ventricular arrhythmias after MI. THIR could have an antiarrhythmic potential through an improvement of electrical coupling.


*Keywords:* Gap junctions; Connexin43; Heavy ion radiaton; Myocardial infarction; Ventricular arrhythmias; Arrhythmia (mechanisms); Epicardial mapping

## 1. Introduction

Modalities currently available for treatment and prevention of life-threatening ventricular tachyarrhythmias (VT/VF) are antiarrhythmic drugs, catheter ablation and implantable cardioverter/defibrillator (ICD). The usefulness of these therapeutic options is limited by either low efficiency, intolerable side

* Corresponding author. Tel.: +81 52 789 3871; fax: +81 52 789 3890.
*E-mail address:* ikodama@riem.nagoya-u.ac.jp (I. Kodama).
[1] The first two authors contributed equally to this work.

0008-6363/$ - see front matter © 2006 European Society of Cardiology. Published by Elsevier B.V. All rights reserved.
doi:10.1016/j.cardiores.2006.09.010